

X-ray Emission from Orion Nebula Cluster Stars with Circumstellar Disks and Jets

Joel H. Kastner¹, Geoffrey Franz¹, Nicolas Grosso², John Bally³, Mark J. McCaughrean⁴, Konstantin Getman⁵, Eric D. Feigelson⁵, Norbert S. Schulz⁶

ABSTRACT

We investigate the X-ray and near-infrared emission properties of a sample of pre-main sequence (PMS) stellar systems in the Orion Nebula Cluster (ONC) that display evidence for circumstellar disks (“proplyds”) and optical jets in Hubble Space Telescope (HST) imaging. Our study uses X-ray data acquired during Chandra Orion Ultradep Program (COUP) observations, as well as complementary optical and near-infrared data recently acquired with HST and the Very Large Telescope (VLT), respectively. Approximately 70% of \sim 140 proplyds were detected as X-ray sources in the 838 ks COUP observation of the ONC, including \sim 25% of proplyds that do not display central stars in HST imaging. In near-infrared imaging, the detection rate of proplyd central stars is $> 90\%$. Many proplyds display near-infrared excesses, suggesting disk accretion is ongoing onto the central, PMS stars. About 50% of circumstellar disks that are detected in absorption in HST imaging contain X-ray sources. For these sources, we find that X-ray absorbing column and apparent disk inclination are well correlated, providing insight into the disk scale heights and metal abundances of UV- and X-ray-irradiated protoplanetary disks.

Approximately 2/3 of the \sim 30 proplyds and PMS stars exhibiting jets in Hubble images have COUP X-ray counterparts. These jet sources display some of the

¹Chester F. Carlson Center for Imaging Science, Rochester Institute of Technology, 54 Lomb Memorial Dr., Rochester, NY 14623; jhk@cis.rit.edu

²Laboratoire d’Astrophysique de Grenoble, Universite Joseph-Fourier, 38041 Grenoble Cedex 9, France

³Center for Astrophysics and Space Astronomy, University of Colorado, 389 UCB, Boulder, CO 80309-0389

⁴University of Exeter, School of Physics, Stocker Road, Exeter EX4 4QL, Devon , UK; and Astrophysikalisches Institut Potsdam, An der Sternwarte 16, 14482 Potsdam, Germany

⁵Department of Astronomy and Astrophysics, Pennsylvania State University, 525 Davey Laboratory, University Park, PA 16802

⁶Center for Space Research, MIT, Cambridge, MA 02139

largest near-infrared excesses among the proplyds, suggesting that the origin of the jets is closely related to ongoing, PMS stellar accretion. One morphologically complex jet source, d181–825, displays a double-peaked X-ray spectral energy distribution with a prominent soft component that is indicative of strong shocks in the jet collimation region. A handful of similar objects also display X-ray spectra that are suggestive of shocks near the jet source. These results support models in which circumstellar disks collimate and/or launch jets from young stellar objects and, furthermore, demonstrate that star-disk-jet interactions may contribute to PMS X-ray emission.

Subject headings: circumstellar matter — ISM: Herbig-Haro objects — open clusters and associations: individual (Orion Nebula Cluster) — planetary systems: protoplanetary disks — stars: pre-main sequence — X-rays: stars

1. Introduction

Some of the best examples of circumstellar disks around low-mass, pre-main sequence (PMS) stars are found among the members of the Orion Nebula Cluster (ONC). These objects, detected in *Hubble Space Telescope* (HST) imaging and dubbed “proplyds” (short for “protoplanetary disks”) by O’Dell and collaborators (O’Dell & Wong 1996 and references therein), are seen in projection in front of (or lie embedded within) the Orion Nebula. The morphologies of proplyds¹ seen in HST imaging range from cometary globules that are externally illuminated and/or ionized to structures resembling dusty disks seen in silhouette against the bright nebular background² (McCaughrean & O’Dell 1996; Bally, O’Dell, & McCaughrean 2000). In addition, many proplyds and other ONC members are observed to drive collimated jets. Such jets are detected on scales ranging from the subarcsecond (“microjets”; Bally et al.) to many arcminutes (Smith et al. 2005; Bally et al. 2005) as a consequence of the emission from ionized gas close to the central stars and of the large-scale chains of knots of shock-excited emission (known as Herbig-Haro [HH] objects) powered by the outflowing gas, respectively.

¹The term proplyd is used throughout this paper to refer to apparent PMS circumstellar disk systems detected in HST imaging, but use of this term is not intended to suggest that the status of such systems as planet formation sites is well established.

²Similar silhouette structures were noted by Feibelman (1989), based on examinations of deep photographs of the Orion Nebula.

The origins of PMS jets are, presumably, intimately related to the presence of circumstellar disks, as present theory holds that these disks provide the jet launching and/or collimation mechanisms (as first proposed by Blandford & Payne [1982] in the context of black hole accretion disks). Several such mechanisms have been proposed to explain PMS jets and outflows, with most of these mechanisms invoking disk and/or stellar magnetic fields (e.g., the so-called “X-wind” model, Shu et al. 1988, 1995; see also Goodson, Winglee, & Boehm 1997; Turner, Bodenheimer, & Rozyczka 1999; Delamarter, Frank, & Hartmann 2000; Matt et al. 2003; a nonmagnetic outflow launching model was proposed by Soker & Regev 2003). Hence, ONC sources exhibiting microjets offer a probe of the disk-jet connection in low-mass, PMS stars.

A key result of the first *Chandra X-ray Observatory* (CXO) observations of the ONC was the detection of a number of X-ray sources at or near the positions of proplyds (Garmire et al. 2000; Schulz et al. 2000). While proplyd X-rays are most readily attributed to magnetic activity associated with their host PMS stars (Feigelson & Montmerle 1999; Favata & Micela 2003), plasma production from magnetic star-disk-jet interactions may also play a role. In this respect, the detection of X-ray emission from proplyds, and further characterization of their X-ray emission properties, should inform the present debate concerning the processes responsible for X-ray emission from low-mass, PMS stars in general (see, e.g., discussions in Kastner et al. 2004 and Preibisch et al. 2005). Furthermore, the attenuation of proplyd X-ray sources by circumstellar material can be used as a unique probe of the density structure of protoplanetary disks and of X-ray irradiation of circumstellar disks by the central T Tauri stars.

Soft and/or diffuse X-ray emission has also been detected in association with several protostellar outflows (e.g., Pravdo et al. 2001, 2004; Favata et al. 2002; Bally et al. 2003; Tsujimoto et al. 2004). Such emission presumably originates from energetic shocks generated by collisions between protostellar jets and ambient molecular cloud material (e.g., Pravdo et al. 2001; Bonito et al. 2004). Despite the frequent association of both jets and X-rays with proplyds, however, it has yet to be established whether any proplyds actually produce X-ray emission via shocks.

On a more fundamental level, the nature of proplyds that lack central stars in HST imaging (Bally et al. 2000) remains uncertain. Although these objects resemble morphologically those proplyds that clearly consist of envelopes and/or disks surrounding low-mass, PMS stars, the PMS evolutionary status of “starless” proplyds has yet to be firmly established. High-resolution X-ray and near-infrared imaging provides an excellent means to determine whether, in fact, such objects contain central, PMS stars.

The Chandra Orion Ultradeep Program (COUP) observation of the ONC (Getman et

al. 2005a) has resulted in the detection of ~ 1400 X-ray emitting PMS stars in the ONC (Getman et al. 2005b), including the majority of previously catalogued proplyds. In this paper, we investigate the X-ray emission and optical/infrared properties of these objects. Images recently acquired with the Advanced Camera for Surveys (ACS) aboard the Hubble Space Telescope (HST) provide improved optical positions for proplyds. These images, in combination with the COUP X-ray data as well as near-infrared photometry acquired with the Very Large Telescope (VLT), yield new insight into the nature of the ONC’s proplyds and jet sources.

In §2 the sample and data are described; §3 contains a description of the results of the correlation of X-ray source positions with optical (HST/ACS) and near-infrared source positions; in §4, results are presented for the X-ray counterparts to circumstellar disks detected in absorption in the ACS images and jet sources, and §5 contains results for the X-ray and near-infrared emission properties of ONC optical jet sources. A discussion of these results is presented in §6. Sec. 7 contains a summary.

2. The Proplyd Sample: HST & COUP Observations

The HST surveys of O’Dell & Wong (1996) and Bally et al. (2000) constitute the basis for our identification of the COUP X-ray counterparts to ONC proplyds. There is considerable overlap between these two surveys, with only four proplyds (159-418, d163-026s, d172-028s, and d244-440) in Bally et al. not included in the lists of O’Dell & Wong (where the proplyd names used here follow the nomenclature of O’Dell & Wen [1994] and Bally et al.). Proplyds 140-512 and 141-520 in O’Dell & Wong (1996) correspond to the single proplyd d141-520 in Bally et al. (2000). After removing such duplications, a total of 164 proplyds, proplyd candidates, and jet (or wind) sources are identified by these two surveys. To this total, we add 7 new proplyds identified in recent HST Advanced Camera for Surveys (ACS) imaging by Smith et al. (2005), and 1 additional proplyd (044-527) identified during the course of our own inspection of the ACS images (§2.2). The complete sample of objects considered here is listed in Tables 1 and 2, where Table 2 includes only those objects that do not appear as proplyds in ACS imaging (§2.2).

2.1. Imaging with the HST Advanced Camera for Surveys

The HST/ACS Wide Field Camera (WFC) images analyzed for this paper constitute a subset of a mosaic, obtained during HST Cycle 12, that covers more than 400 square

arcmin. This ASC Orion image set was obtained through the WFC’s F658N filter, such that the images include $\text{H}\alpha$ $\lambda 6563$ and $[\text{N II}]$ $\lambda 6583$ emission. The pixel scale was $0.05'' \text{ pix}^{-1}$. The images were calibrated astrometrically based on 2MASS imaging of the ONC. These and other aspects of the observations and data reduction are described in detail in Bally et al. (2005; see also Smith et al. 2005).

To verify the identifications of proplyds and jet sources, and to ascertain the precise positions and morphologies of these sources, we examined the ACS images at the position of each of the 166 objects lying within the field of view of the ACS mosaic. A description of the appearance of each proplyd candidate is included in Tables 1 and 2. Generally, the objects listed in Table 1 fall into one or both of two categories, as noted by Bally et al. (2000): (1) dark disks seen in absorption against the bright nebular background, and (2) externally illuminated and/or ionized globules (noted in Table 1 as “cometary rim” or “cometary tail”). As noted in Table 1, some of the proplyds also show evidence for collimated jets and/or teardrop-shaped ionization fronts. The ionization fronts result from photoablation and photoionization of circumstellar material caused by the intense UV fields of the OB stars in the Orion Trapezium cluster.

For $\sim 70\%$ of the proplyds, central stars are apparent in the ACS images. The positions listed in Tables 1 and 2 are the positions of these stars (in the case of the close binaries listed in Table 2, the positions are those of the brighter component). For those objects with no readily identifiable star, the position listed corresponds to the apparent center of the dark lane within and/or center of symmetry of the inner, circularly symmetric portion of a cometary globule (see §3). We estimate — and correlation with COUP source positions (§3) confirms — that the positions listed in Tables 1 and 2 are typically accurate to $\sim 0.2''$. For proplyds with central stars detected in ACS images, the positions are typically accurate to $\sim 0.1''$, i.e., similar to the astrometric uncertainties of the 2MASS Point Source Catalog³.

We found no evidence for proplyd-like structures (such as just described) at a number of positions previously ascribed to non-stellar sources likely to be proplyds (O’Dell & Wong 1996). Most of these positions, which are listed in Table 2, correspond to apparently single stars, close binaries, or Herbig-Haro objects (“HH knots”); in a few cases, there is no source readily apparent at the listed position. We have eliminated these 22 objects from further consideration as proplyds, although we do report their COUP counterparts (§3) in Table 2.

³See <http://spider.ipac.caltech.edu/staff/hlm/2mass/overv/overv.html>

2.2. COUP data

The ~ 838 ks COUP observation of the ONC represents the richest source of X-ray data yet obtained for a young star cluster. A complete description of the observations and of the X-ray data reduction, source detection, spectral and light curve extraction, and spectral fitting procedures is contained in Getman et al. (2005a). The COUP observation resulted in the detection of 1616 individual X-ray sources, with typical formal positional uncertainties of $< 0.3''$ (and often $< 0.1''$). The vast majority of these sources have been unambiguously identified with pre-main sequence stars detected in the optical and/or near-infrared; overall, only $\sim 10\%$ of COUP sources are associated with extragalactic objects, while $\sim 1\%$ are foreground stars (Getman et al. 2005b). In the present paper, we make use of the association of most COUP sources with near-infrared sources detected in subarcsecond VLT imaging in the J ($1.25\ \mu\text{m}$), H ($1.65\ \mu\text{m}$), and K ($2.2\ \mu\text{m}$) bands (McCaughrean et al., in prep.). The resulting photometry has been converted to the 2MASS JHK_s system, and merged with 2MASS and other available near-infrared photometry to include sources for which magnitudes cannot be obtained from the VLT images (due to detector saturation). Typical photometric uncertainties in the merged near-infrared catalog are < 0.1 mag. We also utilize the results of fits of one- or two-component thermal plasma models to COUP X-ray spectra (Getman et al. 2005a). These fits yield estimates of the line-of-sight absorbing column (N_{H}) to and the broadband (0.5 – 8.0 keV) X-ray luminosity of each source.

3. X-ray and Near-infrared Counterparts to Proplyds

We correlated the positions of COUP sources with the ACS positions of all 172 potential proplyds in Tables 1 and 2. Tables 1–4 summarize the results of this ACS vs. COUP position correlation. We find that all of the X-ray counterparts to those proplyds in Table 1 that lie within $\sim 2'$ of the *Chandra* boresight in the COUP image — i.e., for which the *Chandra* ACIS-I image quality is sufficient to determine whether or not a source is extended with respect to the $< 1.0''$ FWHM *Chandra* PSF, without resorting to deconvolution techniques — are point-like.

From the initial set of 105 COUP source positions that lie within $0.4''$ of the ACS positions of the 172 objects in Tables 1 and 2, we calculated median offsets in RA ($+0.017''$) and dec ($+0.043''$) between COUP and ACS positions. We then applied these median offsets to the ACS positions, so as to refine the search for COUP counterparts and to calculate the ACS-COUP offset for each COUP source (this offset is listed under Δ_X in Tables 1 and 2). We also correlated COUP-corrected ACS positions against the near-infrared source positions in the merged VLT catalog, resulting in the identifications of near-infrared counterparts to

proplyds listed in Table 1 (where the ACS-infrared positional offset is given by Δ_I in Table 1).

Table 3 summarizes the optical and X-ray properties of *bona fide* (Table 1) proplyds having COUP counterparts. The listed stellar spectral types and visual extinction data were compiled by Getman et al. (2005a), while the X-ray hardness ratios, absorbing columns ($\log N_H$), and luminosities ($\log L_{t,c}$) were determined by Getman et al. from analysis of the COUP data. The values for $\log N_H$ and $\log L_{t,c}$ have typical formal uncertainties of ~ 0.1 dex; however, the systematic uncertainties — due to, e.g., assumptions adopted in the automated spectral modeling procedure — can be much larger (see discussion in Getman et al. 2005a).

We find the detection fractions of point-like X-ray and near-infrared counterparts to these proplyds are $\sim 66\%$ and $\sim 92\%$, respectively⁴ (Table 4). Table 4 makes clear that proplyds with ACS-detected central stars are detected far more readily in X-rays ($\sim 80\%$ COUP detection rate) than proplyds without visible central stars ($\sim 25\%$ COUP detection rate). This result, of course, is most likely due to the larger absorbing column characteristic of proplyds without optically detected stars. In §4, we elaborate on this result in the context of proplyds that appear to harbor “silhouette disks” (McCaughrean & O’Dell 1996).

The high X-ray detection rate of proplyds in the COUP data is not surprising, in that it is consistent with the status of these objects as low-mass, pre-main sequence stars embedded in circumstellar disks and/or envelopes. The detection by COUP of $\sim 25\%$ of those proplyds that lack optically detected central stars is significant, however, as it indicates that even apparently “starless” proplyds in fact harbor optically obscured PMS stars.

Though it is not a proplyd, one object in Table 2, 155-040, is particularly noteworthy. This object is HH 210, a shocked emission complex that is found at the tip of one of the “fingers” extending radially away from the Kleinmann-Low nebula (Allen & Burton 1993). COUP X-ray source 703 is found at the apex of a bow-shock-like structure in HH 210; as such, it is one of only a handful of COUP sources thus far identified as counterparts to HH objects (Getman et al. 2005b). The implications of the detection of X-ray-emitting gas associated with HH 210 will be considered in detail in Grosso et al. (2005, in prep.).

⁴All of the proplyds listed in Table 1 as not detected (“NV”) in the merged VLT catalog do have near-infrared counterparts, but these counterparts appear nebulous rather than point-like.

3.1. Near-infrared colors of proplyds and jet sources

In Fig. 1 we display a near-infrared (JHK_s) color-color diagram for those COUP sources in Table 1 for which near-infrared photometry is available via the VLT imaging or (in a handful of cases) from 2MASS data (Getman et al. 2005a). The plot includes the JHK_s colors of all COUP sources, for reference. It is apparent that the proplyd sources, as a class, display red $H - K_s$ colors relative to $J - H$. Specifically, whereas the vast majority of the very red COUP X-ray sources lie along the region of $J - H$ vs. $H - K_s$ space that can be attributed to reddening by intervening dust, the colors of the COUP-detected proplyds are indicative of near-infrared excesses. For low-mass, PMS stars, such excesses are commonly attributed to dusty accretion disks and, furthermore, the magnitude of infrared excess appears to be correlated with accretion rate (Meyer et al. 1997). It is therefore noteworthy that the near-infrared colors of the proplyds resemble those of actively accreting (classical) T Tauri stars (Fig. 1). We caution that it is possible that $B\gamma$ emission from ionized gas at the surfaces, photo-ablation winds, and/or jets of some proplyds contaminates the K_s band photometry, mimicking an excess in $H - K_s$. Such an effect probably is not significant for most sources in Fig. 1, however, as we expect that the total contribution from diffuse emission typically should be $< 1\%$ of the total K_s band flux.

4. COUP Sources within Silhouette Disk Proplyds

Certain proplyds exhibit optical absorption morphologies that serve as direct evidence of the presence of dusty, circumstellar disks (see discussions in McCaughrean & O’Dell 1996 and Bally et al. 2000). We find that a total of 39 proplyds appear to harbor (or consist of) such silhouette disks (Table 5). Half of these objects have central stars detected in the visible and/or X-ray regimes, and all but 2 silhouette disk proplyds were detected as point sources in near-infrared imaging (both of these “nondetections,” d154-240 and d182-413, appear as extended sources in the VLT images). The latter, high detection rate confirms that these structures are, in fact, circumstellar disks associated with PMS stars.

ACS images of representative silhouette disks with COUP counterparts (see below) are displayed in Fig. 2. A histogram of the number of such disks vs. apparent aspect ratio (i.e., the apparent disk major to minor axis ratio, as estimated from the ACS images; see Table 5) is presented in Fig. 3. The figure indicates that there the frequency of silhouette disks declines with increasing aspect ratio. Such a relationship would be expected if these objects in fact reflect a population of circularly symmetric disks viewed at random inclinations. This result confirms that the aspect ratio of structures seen in silhouette serves as a direct indicator of disk inclination, as assumed by Bally et al. (2000).

The X-ray detection rate of silhouette disk proplyds is evidently a steep function of disk aspect ratio and, hence, disk inclination (Fig. 3). The effect of disk inclination is also apparent in representative X-ray spectra of sources associated with silhouette disks: X-ray sources that are embedded within more highly inclined silhouette disks generally display harder spectra that are indicative of larger absorbing columns (Fig. 4). This effect is shown more clearly in a plot of $\log N_{\text{H}}$ vs. aspect ratio (Fig. 5). This plot demonstrates that absorbing column increases with increasing aspect ratio, as would be expected if these structures are in fact dusty disks, and those objects with aspect ratios ≥ 3 are viewed nearly edge-on. Indeed, two out of three silhouette disks that include embedded X-ray sources and display aspect ratios ≥ 2.5 have optically undetected central stars (Fig. 5). Furthermore, comparison of Fig. 3 and Fig. 5 indicates that there is a systematic bias against detection of X-ray sources in edge-on (or nearly edge-on) disks, wherein the detection threshold is $\log N_{\text{H}} (\text{cm}^{-2}) \gtrsim 24$.

A few COUP sources associated with silhouette disks warrant special attention, as we now describe.

4.1. Silhouette disks harboring luminous central stars

The proplyds d053-717 and d218-354, both of which are associated with COUP X-ray sources (Table 5), stand out among the high-aspect-ratio silhouette disks as having unusually bright central stars in ACS imaging (Fig. 2). Indeed, the central star of d218-354 is saturated in the ACS image. Nevertheless, it appears that the silhouette disks in both systems are viewed at large inclination, with d053-717 possibly viewed nearly edge-on. The absorbing column of $\log N_{\text{H}}(\text{cm}^{-2}) = 21.67$ that is associated with COUP 1174, the X-ray counterpart to d218-354, is consistent with the value of $A_V = 1.51$ inferred for the coincident optical star, which is estimated to be of late G or early K type.

The X-ray counterpart to d053-717, COUP 241, however, displays a highly absorbed spectrum (Fig. 4) characterized by $\log N_{\text{H}}(\text{cm}^{-2}) = 22.7$. This is far in excess of the N_{H} that would be predicted from the visual absorption of $A_V = 0.43$ inferred from optical/near-infrared photometry of the (mid-K type) central star, assuming standard ISM values of gas-to-dust ratio. It is therefore possible that the circumstellar material in d053-717 is unusually dust-poor. Alternatively, the discrepancy could also be explained if, despite the apparent positional coincidence, the optically luminous central star of d053-717 is not the source of X-ray emission in this system. That is, the X-ray-emitting PMS star may lie embedded within the disk, with the optically detected star as binary companion; this would require that the binary orbit and disk are not coplanar. Finally, it is also possible that the value of A_V toward the central star of d053-717 has been underestimated.

4.2. COUP sources in “starless” silhouette disks

Three COUP sources (419, 476, and 814) are associated with silhouette disks within which no central stars are detected in ACS images. We discuss COUP 476 in §5.

COUP source 419 is particularly noteworthy. This weak source (24 net counts) is the X-ray counterpart of d114-426, which is among the best examples of an apparent edge-on silhouette disk (McCaughrean et al. 1998; Fig. 2). It therefore does not appear to be coincidental that the value of absorbing column determined from the COUP spectrum of this source, $\log N_{\text{H}}(\text{cm}^{-2}) = 23.7$, is the largest of any of the proplyd X-ray counterparts. This source is considered further in §6.1.

The source COUP 814 lies very near the silhouette disk proplyd 166-519, but may be associated with a faint, ACS-detected binary companion rather than with the dark disk. This interpretation is supported by the rather modest column density found for COUP 814 ($\log N_{\text{H}}(\text{cm}^{-2}) = 20.8$) via spectral fitting.

5. COUP X-ray Detections of Jet Sources in the ONC

Among the Table 1 sources are 30 objects exhibiting jet-like structures in either the recently obtained ACS $\text{H}\alpha$ images or in earlier HST narrow-band imagery (Bally et al. 2000). These objects are listed in Table 6. There is considerable overlap with the silhouette disk sample; 8 of these jet sources appear as silhouette disks in the ACS images (Tables 5, 6). Approximately 60% of the jet and “microjet” sources were detected in the COUP X-ray observations (Table 4). Here, we consider in some detail the X-ray emission properties of one of the more remarkable examples of a proplyd disk-jet system, d181-825.

5.1. The Beehive Proplyd

The X-ray source COUP 948 is associated with the Beehive Proplyd, d181-825, which has been described in detail by Bally et al. (2005). This object constitutes one of the most striking examples of a proplyd disk-jet-ionization front system (Fig. 6). An elliptical silhouette disk is evident at the center of the object, and jets are observed to protrude along the minor axis of the ellipse. It is not clear whether the central star is detected directly in the ACS image, given the bright jet emission in close proximity to the apparent position of the central source (perhaps combined with the enhancement of $\text{H}\alpha$ emission, relative to the stellar continuum, by the narrow-band filter used in the ACS imaging). Surrounding this

central disk/jet region is an elegant system of ionization fronts that appears to exhibit a corrugated paraboloid structure. Bally et al. (2005) propose that this structure may trace density waves moving at about the sound speed ($\sim 3 \text{ km s}^{-1}$) in the neutral medium just inside the ionization fronts. These waves likely would be generated by the passage of pulses of supersonic jet ejecta. Such pulses, in turn, are responsible for a series of HH objects and bow shocks that extends several arcmin north and south of d181-825 (Bally et al. 2001, 2005).

The X-ray spectrum of the Beehive source (COUP 948) stands out among the proplyd X-ray sources. This spectrum is clearly double-peaked, consisting of distinct hard and soft components that correspond to thermal plasma at $kT_1 = 0.57 \text{ keV}$ and $kT_2 = 3.55 \text{ keV}$ (Fig. 6). Furthermore, the results of spectral fitting by Getman et al. (2005a) indicate these two components are viewed through very different absorbing columns of $\log N_{\text{H}}(\text{cm}^{-2}) = 20.9$ and $\log N_{\text{H}}(\text{cm}^{-2}) = 22.8$, respectively. The large absorbing column characterizing the hard component suggests this emission is strongly attenuated by gas and dust within the inner regions of the circumstellar disk detected in the ACS imagery. In contrast, the rather small absorbing column toward the soft component suggests that the soft X-rays are subject to little or no attenuation by the circumstellar disk.

To investigate whether the soft X-ray emission is in fact extended (e.g., is generated in the same shocks that are responsible for the HH objects in the system), we carried out spatial deconvolutions of the emission from COUP 948. We find that the emission is point-like, to within the uncertainties. There is marginal evidence for a small ($< 0.2''$) displacement between the hard and soft components, with the centroid of the soft component located slightly south of the centroid of the hard component, in the deconvolved X-ray images.

The light curves of soft (0.5–2.0 keV) and hard (2.0–8.0 keV) X-ray emission from the Beehive are displayed in Fig. 7. Whereas the light curve of the soft component is consistent with a constant count rate, the hard component is clearly variable and displays a strong flare near the end of the COUP observations.

5.2. Potential analogs to the Beehive?

A plot of Chandra/ACIS hardness ratios as measured in the COUP data is presented in Fig. 8, where we include only sources for which hardness ratio uncertainties are ≤ 0.1 (generally, this condition is only met by sources with several hundred counts). This Figure demonstrates that almost all of the proplyd X-ray sources lie along a locus of hardness ratios characteristic of absorbed plasma emission that is dominated by components with $kT > 1$

keV. However — as a consequence of its unusual, double-peaked X-ray spectrum — COUP 948 lies well above this locus.

Only one other well-detected (> 100 net counts) COUP proplyd source lies near COUP 948 in Fig. 8. This source, COUP 1011, is associated with the proplyd 191-350. Like the Beehive, this “cometary globule” proplyd displays well-collimated, bipolar jets in ACS images (Fig. 9). Although not as clearly double-peaked, the X-ray spectrum of COUP 1011 (not shown) somewhat resembles that of COUP 948, resulting in its anomalous hardness ratios.

Among the other COUP counterparts to proplyds that clearly exhibit jets in ACS imaging (Fig. 9), COUP 476 and 524 (X-ray counterparts to the jet sources d124-132 and 131-247, respectively) also appear to have “Beehive-like” hardness ratios (Table 3). However, while COUP 476 appears to display a double-peaked X-ray spectrum, neither source is well detected (less than 50 net counts in each case). This renders their spectral similarity to COUP 948 questionable and, indeed, we have not included these sources in Fig. 8. Another five COUP sources (COUP 279, 693, 747, 900, and 1262, associated with proplyds 069-601, 152-738, d158-327, 176-325, and 236-527, respectively) also display anomalous hardness ratios (Table 3). In each case, however, these sources either suffer from poor photon counting statistics or high background count rates, rendering their hardness ratios unreliable (and these sources therefore are also omitted from Fig. 8). Of these five sources, only COUP 279 — whose spectrum is dominated by a soft component characterized by $kT = 0.71$ keV — appears to be a viable candidate for shock-generated X-ray emission. The associated object detected in ACS imaging, 069-600, appears to be surrounded by a wind collision front (Bally et al. 2000) and may be a microjet source (Fig. 9). We discuss these sources in more detail in a forthcoming paper (Grosso et al. 2005, in prep.).

6. Discussion

The detection of X-ray emission from a very large fraction of Orion Nebula Cluster circumstellar disk sources imaged with the Hubble Space Telescope has a wide range of astrophysical applications. We focus our discussion here on two issues. First, the measurement of increasing soft X-ray absorption as stellar X-rays penetrate longer path lengths through circumstellar disks (Figure 5) constrains the geometries and compositions of such disks (§6.1). Second, X-ray emission from jets which power large-scale outflows (§5) offers insight into conditions around the star-disk-outflow interface (§6.2).

6.1. Disk geometry and composition

The X-ray detections of highly inclined silhouette disks — and, in particular, the measurement of the absorbing column toward COUP 419, the X-ray source detected within the nearly edge-on disk d114-426 — are notable in that they provide unusually clear examples of the X-ray irradiation of T Tauri accretion disks by the central T Tauri stars themselves. These results, coupled with the detection in several COUP sources of fluorescent 6.4 keV line emission that is evidently due to reflection off of circumstellar disks (Tsujimoto et al. 2005), have a variety of implications for physical processes in PMS circumstellar disks. The X-rays absorbed by the disk will affect its ionization, dynamics (particularly degree of turbulence), heating, and chemistry, while flare-produced energetic particles may produce spallogenic nuclear reactions in disk material. Consideration of these issues lies beyond the scope of this paper; readers are referred to reviews by Glassgold et al. (2000, 2005) and Feigelson (2005).

The X-ray-inferred absorbing columns toward COUP 419 and the other silhouette proplyds provide, in principle, the first direct measurements of the gas content of OB photoevaporated protoplanetary disks. To explore this potential, which is manifested in the apparent relationship between silhouette disk orientation (as inferred from ACS imaging) and column density (as inferred from X-ray spectral fitting of COUP counterparts to silhouette disk proplyds), we employ a simple disk density model (Aikawa & Herbst 1999). The Aikawa & Herbst model describes the density of H atoms as a function of radial and vertical displacements within a minimum mass solar nebula (disk) surrounding a star of solar mass and luminosity. The spatial scale of this model, which extends to a radius $R_{\text{out}} \sim 10^3$ AU, is compatible with that of the proplyds in the ACS images. The Aikawa & Herbst model is very similar to that formulated by D’Alessio et al. (1999; see also Glassgold et al. 2004, their Fig. 1). The imposition of hydrostatic equilibrium in these models leads to a flared disk. Such hydrostatic models well describe accretion disks around T Tauri stars for which the dominant source of incident radiation is the central star itself, and for which the gas-to-dust ratios are similar to those typical of the interstellar medium. In employing the Aikawa & Herbst model, we therefore ignore heating and photoionization due to OB star radiation fields (see, e.g., Hollenbach et al. 2000).

We integrated the radial and vertical density distribution of this disk model over a range of disk inclinations i , with inner disk radii (“holes”) ranging from 0.03 AU (i.e., disk extending nearly to the PMS stellar photosphere) to 10 AU, to yield the model dependence of the column density N_{H} on i (Fig. 10). To facilitate comparison with the observed distribution of N_{H} with disk inclination (Fig. 5), we adopt the disk inclination estimates listed in Bally et al. (2000) so as to indicate the approximate positions of three representative proplyds in Fig. 10.

This comparison indicates that, for the specific case of d114-426, the “canonical” T Tauri disk model overestimates (by about two orders of magnitude) the actual proplyd column densities along (within $\sim 10^\circ$ of) the disk plane. However, the same model also vastly underestimates the column densities for disks d218-354 and d172-028, which are viewed at intermediate inclinations. This latter discrepancy suggests that the scale heights of these ONC proplyds are much larger than that assumed in the model. This result would appear to be consistent with the observation that a large fraction of proplyds (i.e., those noted in Table 1 as “cometary” in appearance) are subject to the intense radiation fields of the Trapezium OB stars (O’Dell & Wong 1996; Bally et al. 2000). These fields are rapidly ablating many proplyds, resulting in disk mass loss rates that can exceed $10^{-7} M_\odot \text{ yr}^{-1}$ (Störzer & Hollenbach 1999; Bally et al. 2000). This ablation process is responsible for the cometary globule morphologies that are commonly associated with proplyds, including many of those contained in the silhouette disk sample (Table 1). One would therefore expect the scale heights of silhouette disk proplyds to be systematically larger than those of the “canonical” T Tauri disk model. Such a conclusion is supported by Fig 10 (although we note that neither d218-354 nor d172-028 display clear evidence for ongoing photo-ablation, in the ACS images). In addition, many silhouette disk proplyds in Fig. 5 likely are viewed through large intervening absorbing columns (typically $\sim 2 \times 10^{21} \text{ cm}^{-2}$, corresponding to $A_V \sim 1$; e.g., O’Dell 2001) due to foreground material, such that the discrepancies between model and observations may not be due entirely to the effects of disk ablation. There is also considerable scatter in the X-ray absorption measurements shown in Fig. 5, and it is not clear whether this scatter arises from measurement errors in $\log N_{\text{H}}$ and disk aspect ratios, large variations in foreground extinction (O’Dell 2001), or real differences in disk properties.

The apparent deficit of absorbing material toward the X-ray source COUP 419 in (apparently edge-on) d114-426 is unlikely to be caused by photo-ablation of disk gas, however. Evidently little or no ionizing radiation from the Trapezium reaches d114-426, as it is not surrounded by an ionization front. As a consequence, its scale height may be smaller than those typical of UV-irradiated disks in the ONC, resulting in a large silhouette aspect ratio at somewhat more moderate inclination. Given the highly symmetric optical and near-infrared reflection nebula morphology of 114-426 (McCaughrean et al. 1998), however, it seems unlikely that this proplyd is viewed at an inclination as large as $\sim 10 - 15^\circ$ with respect to the disk plane (as would be suggested by the comparison of its measured N_{H} with the predictions of the simple disk model; Fig 10). If the d114-426 silhouette disk is indeed viewed at an inclination $< 10^\circ$, then its small inferred hydrogen column density (relative to the model) could be due instead to the depletion of neutral metals in the gas phase within the circumstellar disk. Such an interpretation would be consistent with the possibility that this silhouette disk harbors a highly evolved population of large grains (Throop et al. 2001;

Shuping et al. 2003). Although it is likely that many or even most circumstellar disks in the ONC are undergoing a similar process of gas depletion, d114-426 may be somewhat unusual in its apparent advanced degree of disk evolution, given the low X-ray detection rate of stars within silhouette disks that are viewed at similar inclinations (Fig. 3).

Intriguingly, the inferred absorbing column toward the apparent shock zone in the Beehive (COUP 948; §5.1) also points to the possibility of substantial metal depletion in some proplyd *outflows*. The reasoning underlying this conclusion is as follows. The presence of a large radius ionization front surrounding the Beehive Proplyd (and other large proplyds with H α -bright ionization fronts) indicates that the object is embedded in a dense cocoon. The contribution of this cocoon to the foreground N_{H} to the star (and, therefore, the jet collimation and shock zone) is obtained from the estimated electron density at the ionization front. The photo-ablation induced mass-loss rate through such an ionization front should be $\sim 2 \times 10^{-7} M_{\odot} \text{ yr}^{-1}$, assuming quasi-steady, spherically symmetric outflow at a velocity of $\sim 10 \text{ km s}^{-1}$. This implies an absorbing column to the disk (i.e., the source of the flow) of $N_{\text{H}} \sim 1.5 \times 10^{21} \text{ cm}^{-2}$ for a disk radius of 50 AU. Given the likelihood that the outflow speed is even lower, and that we view COUP 948 through an additional foreground column, it thus appears that the modest value of absorption toward the soft X-ray-emitting plasma in COUP 948, $N_{\text{H}} \approx 8 \times 10^{20} \text{ cm}^{-2}$, is best explained as reflecting the depletion of metals in the ablating gas.

6.2. X-ray emission from star-disk-jet interaction regions

The infrared excesses of many proplyds are detected shortward of $\sim 3 \mu\text{m}$ (Fig. 1), indicating that there exists hot dust quite close to the central stars in these objects (see also, e.g., McCaughrean & O’Dell 1996; Hayward & McCaughrean 1997). Indeed, Fig. 1 provides strong evidence that the large-scale, disk-like structures detected in ACS imaging of proplyds (§4) constitute the outer regions of circumstellar disks which, in many if not most cases, extend to within a few stellar radii of the central, PMS stars. This, in turn, suggests that, for many proplyds, accretion onto the central star is ongoing.

Furthermore, the near-infrared excesses of the jet sources are among the most extreme exhibited by the COUP-detected proplyd sample (Fig. 1). The magnitude of these excesses suggests that the Beehive and other jet sources are actively accreting at rates of up to $10^{-6} M_{\odot} \text{ yr}^{-1}$ (Meyer et al. 1997). The inner regions of the accretion disks in sources such as the Beehive likely provide both launching and collimating mechanisms for the observed jets (Goodson et al. 1997; Delamarter et al. 2000; Matt et al. 2003).

Given this context — and the scarcity of examples of X-ray emission from shock-heated gas in collimated protostellar outflows — it is therefore quite significant that at least two COUP counterparts to ONC sources with resolved optical jets (COUP 948 and 1011) display unresolved, soft X-ray spectral components that are indicative of shocks very close to the central stars. In particular, the results presented in §5.1 concerning COUP 948, the X-ray counterpart to the central source in the Beehive Proplyd (d181-825), strongly suggest that its soft X-ray spectral component emanates from energetic shocks at the base of its forward-facing (southeastern-directed) jet. Such an interpretation is consistent with (1) the relatively low temperature characteristic of the soft component, (2) the relatively modest value of $\log N_{\text{H}}(\text{cm}^{-2}) = 20.9$ resulting from spectral fitting of the two-component plasma model, and (3) the constant count rate of the soft component. By analogy with the Beehive, it is likely that the unresolved soft components in COUP 1011 and, possibly, COUP 279, 476, and 524 also are generated via energetic shocks in the jet collimation regions of these PMS star-disk-jet systems.

These definitive and tentative soft X-ray detections join only a handful of previous X-ray detections of shock-heated gas in HH outflows (e.g., HH 2, Pravdo et al. 2001; HH 154, Favata et al. 2002, Bally et al. 2003; HH 80/81, Pravdo et al. 2004). The detection of X-ray-emitting shocks at the *base* of the HH 540 flow from d181-825 appears to be most similar to the case of HH 154 in Taurus (Favata et al. 2002; Bally et al. 2003), and is distinct from HH 2 and HH 80/81, both of which display diffuse X-ray emission at or near the positions of optical (HH) nebulosity lying far from the jet sources. Thus, like the HH 154 X-ray source, the origin of the soft X-rays from d181-825 may be intimately related to the jet launching and/or collimation process (see discussion in Bally et al. 2003).

In contrast, the high temperature and variable flux of the hard X-ray spectral component of COUP 948 indicates that this component arises in plasma that is generated via magnetic reconnection events. The large absorbing column further suggests such events arise deep within the disk, close to the star. Given that the X-ray emission from the vast majority of ONC sources appears to be generated by solar-like coronal activity (Preibisch et al. 2005), a similar mechanism is likely to be responsible for the hard X-rays observed from COUP 948. However, it is also possible that this hard, variable X-ray emission may arise from star-disk interactions that are ultimately responsible for the mass ejections detected in HST imagery and the shocks detected in soft X-rays. Such a hard X-ray production mechanism, which has been predicted theoretically (Hayashi, Shibata, & Matsumoto 1996), was also proposed to explain the coincidence of optical/infrared and X-ray outbursts from V1647 Ori (Kastner et al. 2004; Grosso et al. 2005). By extension, the hard X-ray emission from other proplyds — particularly those with large near-infrared excesses — may be due, in part, to star-disk interactions. Regardless of its origin, however, such high-energy emission will have

a profound effect on the ionization and heating of the inner disk as well as the base of the outflow (e.g., Shang et al. 2002, 2004; Glassgold et al. 2004).

7. Summary

We have used the very deep (838 ks exposure) COUP observations of the ONC, as well as deep near-infrared imaging, to identify and investigate the X-ray and near-infrared counterparts to 166 optically detected objects previously identified as protoplanetary disks (“proplyds”) and/or optical jet sources. Imaging with HST/ACS provides improved coordinates and detailed morphologies for all but a small number of these proplyds. On the basis of the ACS images, we reject 22 objects as lacking obvious protoplanetary disk, jet, or globule structures, resulting in a sample of 143 objects (1 object, d347-1535, lies off both the COUP and near-infrared fields of view). Our main results for the X-ray and near-infrared properties of these objects, and the main conclusions we draw from these results, are as follows.

- The vast majority ($\sim 70\%$) of proplyds are X-ray sources, and an even larger fraction of proplyds ($\geq 90\%$) reveal central stars in near-infrared imaging. Of the ~ 40 proplyds that do not display central stars in high-resolution ACS imaging, only a handful lack both X-ray and near-infrared counterparts. The X-ray and near-infrared observations presented here therefore establish beyond doubt the PMS nature of those proplyds lacking central stars in narrow-band optical imaging.
- In a near-infrared color-color diagram ($J - H$ vs. $H - K_s$), most X-ray-emitting ONC proplyds appear to lie on or near the locus of points defined by classical T Tauri stars in Taurus. Assuming little or no contamination of the near-infrared photometry by emission from ionized gas, this indicates that the central stars of most proplyds are actively accreting T Tauri stars. This result further implies that the protoplanetary disk structures detected on scales of 10’s to 100’s of AU via HST imaging are, in fact, the outermost regions of accretion disks that extend to within a few stellar radii of the central stars.
- Almost 40 proplyds appear as (or contain) “silhouette disks” — i.e., disk-like structures detected in absorption against the bright emission-line background of the Orion Nebula in the ACS images — and $\sim 50\%$ of these silhouette disks harbor X-ray sources. These sources provide clear examples of the irradiation of T Tauri star disks by X-rays emanating from the central T Tauri stars themselves. Such X-ray irradiation likely has a profound effect on the heating and chemistry of the inner disk and outflow regions surrounding T Tauri stars.

- For X-ray sources within silhouette disks, we find that X-ray absorbing column increases with increasing apparent disk inclination. Comparison with a simple model of disk density structure suggests that some dusty disks surrounding T Tauri stars in the ONC have been inflated by the heating and/or ablation resulting from the intense UV fields of the Trapezium OB stars. On the other hand, the absorbing column inferred toward the X-ray source within the (apparently) nearly edge-on disk d114-426 — albeit the largest such column observed among the X-ray-emitting proplyds ($\log N_{\text{H}}(\text{cm}^{-2}) = 23.7$) — is 1–2 orders of magnitude smaller than that expected for an edge-on T Tauri disk. This suggests that the d114-426 disk has undergone substantial gas-phase metal depletion. There is also evidence for metal depletion in the photo-ablation outflow from the Beehive Proplyd (d181-825).
- Approximately 2/3 of the ~ 30 sources that display jets in the ACS images have COUP X-ray counterparts. These jet sources display the largest near-infrared excesses and, hence, accretion rates among the proplyd X-ray sources (again, assuming emission from ionized gas does not significantly affect the near-infrared photometry). This is consistent with models in which the inner, star-disk interaction regions of accretion disks provide the launching as well as collimation mechanisms for protostellar jets.
- One of the most spectacular proplyd jet sources, the Beehive (which is the driving source of an extensive series of HH objects and associated bow shocks), also displays perhaps the most remarkable X-ray spectrum among the proplyds. This spectrum is sharply double-peaked, with a lightly absorbed, constant soft component and heavily absorbed, variable hard component. We identify a handful of additional sources whose X-ray spectra may resemble that of the Beehive’s X-ray counterpart, COUP 948. We interpret the soft X-ray component of COUP 948 (and those of its potential analogs) as evidence of the presence of shocked gas at the base of the forward-facing jet. The hard X-ray emission in COUP 948 and potential analogs is likely due to magnetic reconnection events generated via solar-like coronal activity; alternatively, the hard component may emanate from the same star-disk interaction regions that are responsible for disk launching and collimation.

COUP is supported by Chandra Guest Observer grant SAO GO3-4009A (E. D. Feigelson, PI) as well as by the Chandra ACIS Team contract NAS8-38252. Additional support for the work described in this paper was provided by Chandra Guest Observer grant GO4-5012X to RIT.

Facilities: CXO(ACIS-I)

REFERENCES

Aikawa, Y., & Herbst, E. 1999, *A&A*, 351, 233-246

Allen, D. A. & Burton, M. G. 1993, *Nature* 363, 54

Bally, J., Feigelson, E., & Reipurth, B. 2003, *ApJ*, 584, 843

Bally, J., Johnstone, D., Joncas, G., Reipurth, B., & Mallen-Ornelas, G. 2001, *AJ*, 122, 1508

Bally, J., Licht, D., Smith, N., & Walawender, J. 2005, *AJ*, 129, 355

Bally, J., O'Dell, C.R., & McCaughrean, M.J. 2000, *AJ*, 119, 2959

Bonito, R., Orlando, S., Peres, G., Favata, F., & Rosner, R. 2004, *A&A*, 424, L1

D'Alessio, P., Calvet, N., Hartmann, L., Lizano, S., & Canto, J. 1999, *ApJ*, 527, 893

Delamarter, G., Frank, A., & Hartmann, L. 2000, *ApJ*, 530, 923

Favata, F., & Micela, G. 2003, *SSRv*, 108, 577

Favata, F., Fridlund, C. V. M., Micela, G., Sciortino, S., & Kaas, A. A. 2002, *A&A*, 386, 204

Feibelman, W. 1989, *PASP*, 101, 547

Feigelson, E.D. 2005, in *Cool Stars, Stellar Systems and the Sun 13* (F. Favata & J. Schmitt, eds.), ESA SP, in press

Feigelson, E.D., & Montmerle, T. 1999, *ARA&A*, 37, 363

Garmire, G., Feigelson, E. D., Broos, P., Hillenbrand, L. A., Pravdo, S. H., Townsley, L., & Tsuboi, Y. 2000, *AJ*, 120, 1426

Getman, K., Flaccomio, Broos, P., et al. 2005a, *ApJS* (this issue)

Getman, K., Feigelson, Gross, N., et al. 2005b, *ApJS* (this issue)

Glassgold, A. E., Feigelson, E. D., & Montmerle, T. 2000, in *Protostars and Planets IV* (V. Mannings et al., eds.), Univ. Arizona Press, 429

Glassgold, A. E., Feigelson, E. D., Montmerle, T., & Wolk, S. 2005, in *Chondrites and the Protoplanetary Disk* (A. Krot et al., eds.), Astron. Soc. Pacific, in press

Glassgold, A.E., Najita, J., & Igea, J. 2004, *ApJ*, 615, 972

Goodson, A.P., Winglee, R.M., & Boehm, K.-H. 1997, *ApJ*, 489, 199

Grosso, N., et al. 2005, *A&A*, in press

Hayward, T. L., & McCaughrean, M. J. 1997, *AJ*, 113, 346

Hollenbach, D. J., Yorke, H. W., & Johnstone, D. 2000, in *Protostars and Planets IV* (Tucson: University of Arizona Press), eds. V. Mannings, A.P. Boss, S.S. Russell, p. 401

Hayashi, M., Shibata, K., & Matsumoto, R. 1996, *ApJ*, 468, L37

Kastner, J.H., et al. 2004, *Nature*, 430, 429

Matt, S., Winglee, R., & Boehm, K.-H. 2003, *MNRAS*, 345, 660

McCaughrean, M.J., & O'Dell, C.R. 1996, *AJ* 111, 1977

McCaughrean, M.J., et al. 1998, *ApJ*, 492, L157

Meyer, M.R., Calvet, N., & Hillenbrand, L.A. 1997, *AJ*, 114, 288

O'Dell, C. R., & Wen, Z. 1994, *ApJ*, 436, 194

O'Dell, C. R., & Wong, K. 1996, *AJ*, 111, 846

O'Dell, C. R. 2001, *ARA&A*, 39, 99O

Pravdo, S. H., Feigelson, E. D., Garmire, G., Maeda, Y., Tsuboi, Y., & Bally, J. 2001, *Nature*, 413, 708

Pravdo, S. H., Maeda, Y., & Tsuboi, Y. 2004, *ApJ*, 605, 259

Preibisch, T., et al. 2005, *ApJS* (this issue)

Schulz, N. S.; Canizares, C., Huenemoerder, D., Kastner, J. H., Taylor, S. C., & Bergstrom, E. J. 2000, *ApJ*, 549, 441

Shuping, R.Y., Bally, J., Morris, M., & Throop, H. 2003, *ApJ*, 587, L109

Shang, H., Glassgold, A. E., Shu, F. H., & Lizano, S. 2002, *ApJ*, 564, 853

Shang, H., Lizano, S., Glassgold, A. E., & Shu, F. H. 2004, *ApJ*, 612, L69

Shu, F. H., Lizano, S., Ruden, S. P., & Najita, J. 1988, *ApJ*, 328, L19

Shu, F. H., Najita, J., Ostriker, E. C., & Shang, H. 1995, *ApJ*, 455, L155

Smith, N., Bally, J., Licht, D., & Walawender, J. 2005, *AJ*, 129, 382

Soker, N., & Regev, O. 2003 *A&A*, 406, 603

Störzer, H., & Hollenbach, D. 1999, *ApJ*, 515, 669

Throop, H.B., Bally, J., Esposito, L.W., & McCaughrean, M.J. 2001, *Science*, 292, 1686

Tsujimoto, M., Koyama, K., Kobayashi, N., Saito, M., Tsuboi, Y., & Chandler, C. J. 2004, *PASJ*, 56, 341

Tsujimoto, M., et al. 2005, *ApJS* (this issue)

Turner, N. J., Bodenheimer, P., & Rozyczka, M. 1999, *ApJ*, 524, 129

Table 1. Orion Nebula Cluster Proplyds

Proplyd ^a	α^b	δ^b	VLT ^c	Δ_I^d ($''$)	COUP ^e	Δ_X^f ($''$)	Star? ^g	Appearance in ACS image
4596-400	05:34:59.56	-05:24:00.3	137	0.06	Y	I-front ^h
005-514	05:35:00.47	-05:25:14.3	147	0.14	Y	cometary rim, I-front
044-527 ⁱ	05:35:04.43	-05:25:27.4	55	0.20	NC	...	N	cometary rim
d053-717	05:35:05.41	-05:27:17.2	241	0.12	Y?	dark (edge-on?) disk, companion
064-705	05:35:06.42	-05:27:04.7	266	0.14	Y	0.2'' sep. double star
066-652	05:35:06.60	-05:26:52.0	275	0.79	Y	0.2'' sep. double star, bright rim
069-600	05:35:06.91	-05:26:00.7	131	0.26	279	0.22	Y	jet?, wind collision front
d072-135	05:35:07.20	-05:21:34.4	137	0.11	NC	...	N	dark disk, cometary rim
073-227	05:35:07.27	-05:22:26.6	141	0.18	283	0.02	Y	rim?
097-125	05:35:09.68	-05:21:24.9	197	0.04	336	0.31	Y	rim?
102-233	05:35:10.14	-05:22:32.7	214	0.18	358	0.13	Y	cometary rim
102-021	05:35:10.19	-05:20:21.1	216	0.14	362	0.17	Y	cometary rim
106-156	05:35:10.57	-05:21:56.3	243	0.09	382	0.20	Y	cometary rim
106-417	05:35:10.54	-05:24:16.7	242	0.09	385	0.03	Y?	compact nebula, I-front
d109-247	05:35:10.90	-05:22:46.4	261	0.14	403	0.06	Y	cometary rim
d109-327	05:35:10.94	-05:23:26.6	NV	...	NC	...	N	dark disk?, cometary rim
109-449	05:35:10.94	-05:24:48.7	262	0.12	404	0.07	Y?	compact nebula
d110-3035	05:35:10.99	-05:30:35.2	NC	...	N	bipolar jet/nebula
d114-426	05:35:11.31	-05:24:26.4	277	0.14	419	0.17	N	dark disk
117-025	05:35:11.72	-05:20:25.1	NV	...	NC	...	N?	amorphous
d117-352	05:35:11.72	-05:23:51.8	298	0.13	443	0.12	N	cometary rim
119-340	05:35:11.90	-05:23:39.9	NV	...	NC	...	N	cometary rim
d121-192	05:35:12.09	-05:19:24.8	460	0.25	Y	dark disk
121-434	05:35:12.12	-05:24:33.9	316	0.10	465	0.06	N	cometary rim
d124-132	05:35:12.38	-05:21:31.5	325	0.06	476	0.16	N	dark disk, jet?, cometary rim
131-046	05:35:13.06	-05:20:45.9	355	0.14	NC	...	N	dark disk?, cometary rim
131-247	05:35:13.10	-05:22:47.3	359	0.24	524	0.11	N	bright jet, cometary rim
d132-042	05:35:13.24	-05:20:41.9	366	0.15	NC	...	N?	dark disk, jet, cometary rim
d132-183	05:35:13.23	-05:18:33.0	NC	...	N?	dark disk
d135-220	05:35:13.51	-05:22:19.6	380	0.21	551	0.11	Y	cometary rim
138-207	05:35:13.79	-05:22:07.1	396	0.03	579	0.11	Y	cometary rim
139-320	05:35:13.92	-05:23:20.2	405	0.09	593	0.06	N	cometary rim
140-1952	05:35:14.05	-05:19:52.1	410	0.13	597	0.12	Y	dark halo
d141-520	05:35:14.05	-05:25:20.4	411	0.12	604	0.14	Y	dark disk, cometary rim
d141-301	05:35:14.15	-05:23:01.1	NC	...	Y?	(saturated?), cometary rim, dark interior
143-425	05:35:14.26	-05:24:24.8	422	0.15	616	0.20	Y	I-front, no proplyd?
d143-522	05:35:14.34	-05:25:22.2	427	0.29	NC	...	N	dark disk, cometary rim
144-334	05:35:14.38	-05:23:33.7	432	0.25	631	0.20	Y	I-front?, no proplyd
d147-323	05:35:14.72	-05:23:23.0	453	0.16	658	0.11	Y	dark disk, cometary rim
150-231	05:35:15.02	-05:22:31.1	476	0.19	678?	1:	Y	cometary rim
152-319	05:35:15.20	-05:23:18.9	490	0.19	690	0.11	N	cometary rim
152-738	05:35:15.21	-05:27:37.8	693	0.45	Y	I-front?
153-1902	05:35:15.35	-05:19:02.2	695	0.13	Y	compact nebula
154-324	05:35:15.35	-05:23:24.2	502	0.19	NC	...	Y	jet, no proplyd
154-225	05:35:15.37	-05:22:25.4	505	0.21	699	0.17	Y	cometary rim

Table 1—Continued

Proplyd ^a	α^b	δ^b	VLT ^c	Δ_I^d ($''$)	COUP ^e	Δ_X^f ($''$)	Star? ^g	Appearance in ACS image
d154-240	05:35:15.38	-05:22:40.0	NV	...	NC	...	N	dark disk?, cometary rim
d155-338	05:35:15.52	-05:23:37.5	513	0.04	717	0.11	Y	(saturated), cometary rim
156-403	05:35:15.61	-05:24:03.1	522	0.10	726	0.08	Y	(saturated), no proplyd?
157-533	05:35:15.67	-05:25:33.1	525	0.13	728	0.16	Y	(saturated), cometary rim
157-323	05:35:15.72	-05:23:22.5	531	0.12	733	0.12	Y	(saturated)
d158-326	05:35:15.79	-05:23:26.7	537	0.12	NC	...	Y	(saturated), cometary tail
d158-327	05:35:15.84	-05:23:25.6	543	0.11	747	0.07	Y	(saturated), cometary tail
158-323	05:35:15.83	-05:23:22.5	542	0.25	746	0.13	Y	(saturated), cometary tail
159-338	05:35:15.90	-05:23:38.0	549	0.04	757	0.12	Y	(saturated), cometary tail
d159-418	05:35:15.90	-05:24:17.8	550	0.13	748	0.88	N	cometary rim
159-350	05:35:15.95	-05:23:50.0	551	0.04	758	0.15	Y	(saturated), cometary rim
160-353	05:35:16.00	-05:23:53.1	559	0.15	768	0.15	Y	(saturated), cometary rim
161-324	05:35:16.06	-05:23:24.4	564	0.19	NC	...	Y	(saturated), cometary tail
d161-328	05:35:16.07	-05:23:27.9	566	0.17	NC	...	Y?	cometary tail
161-314	05:35:16.10	-05:23:14.3	571	0.17	779	0.18	Y?	fuzzy
163-317	05:35:16.28	-05:23:16.6	585	0.20	787	0.03	Y	(saturated), cometary tail
d163-026 ^j	05:35:16.29	-05:20:25.5	588	0.27	NC	...	N	dark disk, binary?
d163-222	05:35:16.30	-05:22:21.6	590	0.26	799	0.27	Y	dark disk, cometary rim
163-249	05:35:16.33	-05:22:49.1	592	0.25	800	0.16	Y	cometary tail
164-511	05:35:16.36	-05:25:09.6	593	0.07	803	0.16	Y	jet?
165-235	05:35:16.48	-05:22:35.2	602	0.23	807	0.12	Y	cometary rim
d165-254	05:35:16.54	-05:22:53.7	605	0.16	NC	...	N	dark disk
166-519	05:35:16.58	-05:25:17.7	607	0.08	814 ^k	0.18	N?	dark disk?, binary?
166-250	05:35:16.59	-05:22:50.4	NV	...	NC	...	N	cometary tail
166-316	05:35:16.61	-05:23:16.2	611	0.22	820	0.17	Y	(saturated)
d167-231	05:35:16.73	-05:22:31.3	618	0.20	825	0.04	Y	dark disk
167-317	05:35:16.75	-05:23:16.2	619	0.18	826	0.24	Y	(saturated), cometary tail?
168-328	05:35:16.76	-05:23:28.1	622	0.22	827	0.06	Y	(saturated), cometary tail
168-235	05:35:16.83	-05:22:34.6	NV	...	NC	...	N	cometary rim
168-326	05:35:16.84	-05:23:26.3	626	0.17	NC	...	Y	(saturated), cometary tail
169-338	05:35:16.88	-05:23:38.1	NV	...	NC	...	Y	cometary tail
d170-249	05:35:16.97	-05:22:48.7	638	0.21	844	0.22	N	cometary rim
170-337	05:35:17.00	-05:23:37.1	640	0.17	847	0.36	Y	(saturated), cometary tail
d171-340	05:35:17.05	-05:23:39.8	644	0.21	856	0.10	Y	cometary rim
171-334	05:35:17.06	-05:23:34.1	645	0.21	855	0.05	Y	(saturated)
d172-028	05:35:17.22	-05:20:27.7	654	0.11	865	0.10	Y	dark disk?
173-341	05:35:17.32	-05:23:41.5	658	0.22	NC	...	Y	cometary tail
d174-236	05:35:17.34	-05:22:35.8	661	0.32	876	0.14	Y	(saturated), cometary rim
174-414	05:35:17.39	-05:24:13.7	668	0.20	887	0.29	Y	cometary tail
175-251	05:35:17.48	-05:22:51.4	674	0.18	884	0.10	Y	cometary tail
d175-355	05:35:17.54	-05:23:55.1	681	0.11	NC	...	N	compact rim
d176-543	05:35:17.55	-05:25:42.7	679	0.19	901	0.13	Y	dark disk, jet, cometary rim
176-325	05:35:17.55	-05:23:24.9	683	0.28	900	0.22	Y	(saturated), cometary rim
d177-341	05:35:17.67	-05:23:40.9	693	0.23	NC	...	Y	(saturated), cometary rim
177-454	05:35:17.69	-05:24:53.9	694	0.16	914	0.25	Y	bright rim

Table 1—Continued

Proplyd ^a	α^b	δ^b	VLT ^c	Δ_I^d ($''$)	COUP ^e	Δ_X^f ($''$)	Star? ^g	Appearance in ACS image
d177-541	05:35:17.71	-05:25:40.8	695	0.14	NC	...	N	dark disk, cometary rim
177-444	05:35:17.73	-05:24:43.6	697	0.11	NC	...	Y	cometary tail
d179-353	05:35:17.96	-05:23:53.6	720	0.16	NC	...	N	cometary tail
180-331	05:35:18.04	-05:23:30.8	726	0.19	NC	...	N	cometary tail
d181-247	05:35:18.08	-05:22:47.1	729	0.20	NC	...	N	dark disk, cometary tail
d181-825	05:35:18.10	-05:28:25.0	948	0.15	N?	jet, dark disk, I front; Beehive Proplyd
d182-332	05:35:18.19	-05:23:31.6	731	0.16	NC	...	Y?	dark disk
d182-413	05:35:18.22	-05:24:13.4	NV	...	NC	...	N	dark disk, cometary rim
182-316	05:35:18.24	-05:23:15.7	738	0.21	955	0.12	Y	cometary tail?
183-439	05:35:18.28	-05:24:38.7	739	0.20	NC	...	Y	cometary tail; faint companion
d183-419	05:35:18.31	-05:24:18.8	743	0.20	NC	...	N	dark disk, cometary rim
d183-405	05:35:18.33	-05:24:04.7	746	0.17	966	0.22	Y	dark disk
184-427	05:35:18.35	-05:24:26.7	749	0.27	967	0.36	Y	cometary rim; faint companion
184-520	05:35:18.45	-05:25:19.2	753	0.13	NC	...	Y	cometary rim, nebulosity
189-329	05:35:18.87	-05:23:28.9	776	0.16	1000	0.01	Y	cometary tail?
191-350	05:35:19.07	-05:23:49.5	788	0.15	1011	0.27	Y	jet?, nebulosity
d191-232	05:35:19.125	-05:22:31.4	794	0.16	NC	...	N	dark disk
d197-427	05:35:19.66	-05:24:26.4	813	0.23	1045	0.27	Y	dark disk, cometary rim
198-222	05:35:19.82	-05:22:21.6	819	0.18	1056	0.09	Y	cometary rim
198-448	05:35:19.84	-05:24:47.8	820	0.17	1058	0.17	Y	cometary rim
201-534	05:35:20.15	-05:25:33.7	839	0.19	NC	...	Y	jet?
202-228	05:35:20.15	-05:22:28.3	840	0.13	1084	0.07	Y	dark disk, cometary rim
d203-504	05:35:20.27	-05:25:03.9	847	0.24	1091	0.10	Y	cometary rim
d203-506	05:35:20.32	-05:25:05.5	849	0.22	NC	...	N	dark disk
205-330	05:35:20.46	-05:23:29.7	855	0.38	1101	0.18	Y	cometary rim; companion?
205-052	05:35:20.52	-05:20:52.1	859	0.08	1104	0.04	Y	cometary rim
d205-421	05:35:20.54	-05:24:20.8	861	0.15	1107	0.15	Y	dark disk, cometary rim
d206-446	05:35:20.63	-05:24:46.3	864	0.24	1112	0.22	Y	dark disk, cometary rim
208-122	05:35:20.84	-05:21:21.5	876	0.14	1120	0.02	Y	jet?
212-557	05:35:21.16	-05:25:56.9	892	0.26	1139	0.19	Y	irreg. nebula
212-260	05:35:21.24	-05:22:59.5	896	0.14	1141	0.04	Y	cometary tail
213-346	05:35:21.31	-05:23:46.0	901	0.06	1149	0.90	Y	cometary tail
215-317	05:35:21.51	-05:23:16.6	907	0.14	1155	0.27	...	[off ACS FOV]
d216-0939	05:35:21.57	-05:09:38.9	[off ACS FOV]
218-339	05:35:21.77	-05:23:39.2	920	0.04	1167	0.21	Y	cometary tail
d218-354	05:35:21.81	-05:23:53.7	922	0.09	1174	0.27	Y	dark disk
d218-529	05:35:21.83	-05:25:28.3	924	0.25	NC	...	N	dark disk, jet, cometary rim?
221-433	05:35:22.09	-05:24:32.7	932	0.19	1184	0.16	Y	cometary rim
224-728	05:35:22.38	-05:27:28.3	1206	0.13	Y	cometary rim
228-548	05:35:22.83	-05:25:47.5	968	0.26	NC	...	Y	cometary tail
231-502	05:35:23.16	-05:25:02.2	978	0.20	NC	...	Y?	compact nebula
232-453	05:35:23.21	-05:24:52.8	983	0.32	NC	on CCD bleed artifact
236-527	05:35:23.60	-05:25:26.4	1000	0.22	1262	0.19	Y	cometary tail
237-627	05:35:23.66	-05:26:27.0	1004	0.22	1263	0.25	Y	cometary rim
d239-334 ^j	05:35:23.87	-05:23:34.0	1015	0.78	NC	[off ACS FOV]

Table 1—Continued

Proplyd ^a	α^b	δ^b	VLT ^c	Δ_I^d ($''$)	COUP ^e	Δ_X^f ($''$)	Star? ^g	Appearance in ACS image
239-510	05:35:23.98	-05:25:09.8	1021	0.20	1275	0.18	Y	compact nebula
240-314	05:35:24.05	-05:23:13.8	1022	0.32	1276	0.42	..	[off ACS FOV]
242-519	05:35:24.26	-05:25:18.6	1027	0.21	1281	0.20	Y	cometary tail
d244-440	05:35:24.44	-05:24:39.8	1033	0.07	1290	0.15	Y	giant cometary proplyd
245-632	05:35:24.46	-05:26:31.4	1035	0.23	1291	0.04	Y	cometary rim
245-502	05:35:24.51	-05:25:01.5	1038	0.14	1293	0.44	Y	cometary tail
247-436	05:35:24.70	-05:24:35.6	1046	0.13	1302	0.18	Y	cometary rim, jet
250-439	05:35:25.03	-05:24:38.4	1055	0.13	1313	0.12	Y	cometary tail
d252-457	05:35:25.21	-05:24:57.2	1060	0.16	1317	0.24	Y	cometary rim, jet
d253-1536 ^j	05:35:25.30	-05:15:35.5	NC	...	Y?	dark disk, jets
264-532	05:35:26.42	-05:25:31.5	1096	0.19	NC	[off ACS FOV]
d280-1720	05:35:28.04	-05:17:20.2	1404	0.24	Y	dark disk
282-458	05:35:28.21	-05:24:58.2	1144	0.01	1409	0.15	...	[off ACS FOV]
d294-606	05:35:29.48	-05:26:06.6	1164	0.11	NC	...	N	dark disk
d347-1535	05:35:34.67	-05:15:34.8	N	dark disk, bipolar jet

^aProplyd candidates with prefix “d” are from lists in Bally et al. (2000) or Smith et al. (2004); all other candidates are from O’Dell & Wong (1996).

^bJ2000 coordinates determined from ACS images; for sources outside ACS FOV, coordinates are from Bally et al. (2000), Smith et al. (2004), or O’Dell & Wong (1996). See text.

^cVLT IR source number. The text “NV” indicates no IR counterpart detected; ellipsis indicate candidates lying outside the VLT image FOV.

^dOffset (arcsec) between visual position (as determined from ACS image) and infrared source position.

^eCOUP X-ray source number. The text “NC” indicate no X-ray counterpart detected; ellipsis indicate candidates lying outside the COUP FOV.

^fOffset (arcsec) between visual position (as determined from ACS image) and X-ray source position.

^gY = star apparent in ACS image; N = no star apparent in ACS image

^h“I-front”: ionization front apparent.

ⁱProplyd 044-527 is a new identification.

^jd163-026s is found $\sim 0.4''$ from COUP 796 (= MLLA-956) and d239-334 is found $\sim 0.6''$ from COUP 1268 (= MLLA-347), but optical/IR sources near these proplyds are in fact the X-ray sources; see Fig. 7 of Bally et al. (2000). In addition, COUP 1316 lies at a companion to d253-1536.

^kCOUP 814 lies very near the position of 166-519, but may instead be associated with a companion. See §4.2.

Table 2. Objects Not Considered Proplyds

Object	α^a	δ^a	COUP ^b	Δ^c ($''$)	Comments
113-153	05:35:11.35	-05:21:53.1	HH knot(s)
114-155	05:35:11.44	-05:21:54.8	HH knot(s)
115-155	05:35:11.55	-05:21:54.5	HH knot(s)
116-156	05:35:11.59	-05:21:55.8	HH knot(s)
127-711	05:35:12.71	-05:27:10.7	498	0.05	double star
128-044	05:35:12.81	-05:20:43.6	501	0.06	triple star
132-221	05:35:13.17	-05:22:21.3	523	0.20	double star
132-222	05:35:13.26	-05:22:21.8	no source in ACS image
135-227	05:35:13.47	-05:22:27.0	no source in ACS image
137-222	05:35:13.73	-05:22:22.0	573	0.14	star
144-522	05:35:14.41	-05:25:21.5	no source in ACS image
149-329	05:35:14.92	-05:23:29.1	671	0.20	star (saturated?)
153-321	05:35:15.35	-05:23:21.4	star
154-042	05:35:15.45	-05:20:41.9	HH knot(s)
155-040	05:35:15.49	-05:20:40.1	703	n/a	HH knot(s)
158-425	05:35:15.77	-05:24:24.8	736	0.08	star
169-549	05:35:16.90	-05:25:49.1	no source in ACS image
172-327	05:35:17.22	-05:23:26.7	part of WC front?
174-400	05:35:17.38	-05:24:00.3	880	0.10	star
179-536	05:35:17.90	-05:25:35.9	no source in ACS image
187-314	05:35:18.66	-05:23:14.0	986	0.05	double star
222-637	05:35:22.20	-05:26:37.4	1202	0.11	double star

^aJ2000 coordinates, as determined from ACS images.^bCOUP source number.^cOffset (arcsec) between visual position (as determined from ACS image) and COUP X-ray source position.

Table 3. Proplyds with COUP Counterparts: Optical and X-ray Properties

Proplyd	Sp. Type ^a	A_V (mag)	COUP	Exp. ^b (ks)	Counts ^c	HR2 ^d	HR3 ^e	$\log N_H^f$ (cm ⁻²)	$\log L_{t,c}^g$ (erg s ⁻¹)
4596-400	M2.5-M4	1.03	137	817.0	501	-0.15 ± 0.05	-0.16 ± 0.06	22.0	29.6
005-514	K6e	0.48	147	779.8	2348	-0.60 ± 0.02	-0.34 ± 0.04	21.3	29.9
d053-717	K5-K6	0.43	241	806.4	314	0.65 ± 0.08	0.30 ± 0.06	22.7	29.9
064-705	266	760.4	831	-0.75 ± 0.02	-0.36 ± 0.08	21.2	29.4
066-652	M4.5e	0.47	275	813.4	134	-0.76 ± 0.06	-0.97 ± 0.33	21.7	29.0
069-601	279	565.9	34	-0.95 ± 0.11	0.64 ± 0.68	21.9	28.6
073-227	M2-M4:	0.60	283	778.1	3785	-0.58 ± 0.01	-0.19 ± 0.03	21.1	30.1
097-125	M3.5	...	336	822.3	309	-0.74 ± 0.07	-0.13 ± 0.22	21.6	29.1
102-233	358	344.8	93	0.33 ± 0.12	-0.25 ± 0.12	22.6	30.0
102-021	M3.5	...	362	809.9	220	-0.38 ± 0.07	-0.40 ± 0.12	21.9	29.2
106-156	K2-M2	0.42	382	831.1	5065	-0.63 ± 0.01	-0.38 ± 0.03	21.3	30.2
106-417	K:	...	385	838.2	885	0.63 ± 0.04	0.36 ± 0.03	22.6	30.2
d109-247	mid-K::	...	403	334.2	456	0.47 ± 0.07	0.36 ± 0.05	22.5	30.2
109-449	M3e	...	404	838.2	2413	-0.44 ± 0.02	-0.27 ± 0.03	21.7	30.1
d114-426	419	831.1	24	...	0.96 ± 0.15	23.7	30.2
d117-352	443	785.1	32	0.23 ± 0.26	-0.04 ± 0.23	21.8	28.3
d121-192	M4.5	5.83	460	799.3	349	-0.42 ± 0.05	-0.44 ± 0.09	21.6	29.2
121-434	465	772.8	35	-0.32 ± 0.19	-0.22 ± 0.32	21.6	28.2
124-132	476	827.6	47	-0.68 ± 0.23	0.71 ± 0.22	20.0	28.2
131-247	K:	...	524	834.7	32	-0.19 ± 0.34	0.57 ± 0.19	22.4	28.5
d135-220	M1.4	1.34	551	832.9	654	-0.56 ± 0.03	-0.42 ± 0.07	21.6	29.5
138-207	K2e-M4	...	579	831.1	7100	-0.32 ± 0.01	-0.04 ± 0.02	21.7	30.6
139-320	593	578.3	329	-0.64 ± 0.05	-0.34 ± 0.12	21.3	29.2
140-1952	late-G	2.69	597	804.6	8523	-0.73 ± 0.01	-0.33 ± 0.02	20.0	30.3
d141-520	604	834.7	305	-0.52 ± 0.05	-0.51 ± 0.10	21.2	28.9
143-425	K4-M1	1.24	616	535.8	1096	-0.63 ± 0.02	-0.38 ± 0.06	21.3	29.7
144-334	M1	1.54	631	452.7	1990	-0.52 ± 0.02	-0.33 ± 0.04	21.5	30.1
d147-323	M3e	...	658	834.7	2541	0.18 ± 0.03	0.03 ± 0.02	22.2	30.4
150-231	678	832.9	614	0.63 ± 0.15	0.81 ± 0.03	22.9	30.3
152-319	690	834.7	71	0.52 ± 0.29	0.56 ± 0.11	22.7	29.3
152-738	693	806.4	38	-0.43 ± 0.47	0.85 ± 0.14	23.2	29.5
153-1902	M4.5-M5.5	...	695	792.2	637	-0.76 ± 0.03	-0.55 ± 0.12	20.0	29.1
154-225	M0-M3	...	699	831.1	370	-0.42 ± 0.05	-0.41 ± 0.08	21.6	29.5
d155-338	717	836.4	93	-0.39 ± 0.11	-0.37 ± 0.19	21.0	28.5
156-403	K8-M0	0.81	726	295.3	466	-0.68 ± 0.04	-0.40 ± 0.10	21.4	29.6
157-533	K8e-M0	1.71	728	832.9	190	-0.04 ± 0.09	-0.04 ± 0.09	22.0	29.1
157-323	733	834.7	41	0.51 ± 0.53	-0.13 ± 0.24	22.5	29.4
d158-327	747	834.7	48	-0.20 ± 0.48	0.62 ± 0.22	22.3	28.9
158-323	K1-midKe	...	746	834.7	52	-0.08 ± 0.35	0.14 ± 0.26	22.1	28.8
159-338	757	836.4	25	-0.02 ± 0.29	-0.26 ± 0.33	22.5	29.0
159-350	G5-K0e	3.78	758	788.7	20627	-0.31 ± 0.01	-0.15 ± 0.01	21.7	31.1
160-353	F2-F7e	4.33	768	687.9	1530	-0.33 ± 0.03	-0.18 ± 0.04	21.5	30.3
161-314	779	834.7	93	0.45 ± 0.44	0.07 ± 0.17	22.1	29.1
163-317	K0-K7	...	787	834.7	1115	0.35 ± 0.07	-0.03 ± 0.04	22.4	30.2
d163-222	$\geq M2$...	799	831.1	18	-0.80 ± 0.25	...	21.2	27.8

Table 3—Continued

Proplyd	Sp. Type ^a	A_V (mag)	COUP	Exp. ^b (ks)	Counts ^c	HR2 ^d	HR3 ^e	$\log N_H$ ^f (cm ⁻²)	$\log L_{t,c}$ ^g (erg s ⁻¹)
163-249	M1.5e	2.24	800	832.9	48	0.15 ± 0.28	-0.17 ± 0.25	22.4	28.9
164-511	M1.5	2.26	803	832.9	3535	-0.40 ± 0.02	-0.15 ± 0.03	21.6	30.2
165-235	M4	1.44	807	831.1	1447	-0.56 ± 0.02	-0.30 ± 0.05	21.4	29.7
166-519	M2	2.34	814	832.9	207	-0.60 ± 0.06	-0.57 ± 0.14	20.8	28.7
166-316	820	834.7	152	...	0.50 ± 0.10	22.9	30.1
d167-231	M4	0.41	825	831.1	3641	-0.43 ± 0.02	-0.17 ± 0.03	21.6	30.2
167-317	G4-K5	...	826	834.7	1585	0.05 ± 0.04	0.07 ± 0.03	22.1	30.4
168-328	827	834.7	812	-0.18 ± 0.04	-0.58 ± 0.06	22.2	30.5
d170-249	K5-M2	...	844	831.1	227	-0.26 ± 0.08	-0.45 ± 0.11	22.1	29.2
170-337	M2e	...	847	834.7	216	-0.61 ± 0.06	-0.30 ± 0.14	21.6	29.2
d171-340	K8e	...	856	834.7	3313	-0.43 ± 0.02	-0.31 ± 0.03	21.7	30.3
171-334	K0-K2	2.47	855	834.7	3364	-0.06 ± 0.02	-0.02 ± 0.02	21.7	31.8
d172-028	M3	...	865	811.7	335	-0.50 ± 0.05	-0.44 ± 0.10	21.4	29.0
d174-236	G4-K5	...	876	829.4	253	0.46 ± 0.12	0.44 ± 0.06	22.7	29.8
174-414	M5	2.39	887	581.8	229	-0.51 ± 0.06	-0.45 ± 0.12	21.8	29.3
175-251	884	831.1	244	0.57 ± 0.40	0.79 ± 0.05	23.0	29.9
d176-543	K8	2.48	901	829.4	2303	-0.29 ± 0.02	-0.12 ± 0.03	21.4	30.0
176-325	900	832.9	22	-0.20 ± 0.68	0.61 ± 0.33	23.5	30.4
177-454	M5.5e	1.52	914	390.8	412	-0.71 ± 0.04	-0.43 ± 0.10	21.4	29.5
d181-825	M1:e	0.34	948	795.8	487	-0.28 ± 0.06	0.49 ± 0.05	20.9	30.0
182-316	M2	3.75	955	831.1	170	-0.24 ± 0.09	-0.21 ± 0.12	21.5	28.8
d183-405	M3	2.55	966	783.4	1336	-0.73 ± 0.02	-0.36 ± 0.06	21.7	30.6
184-427	M2.5	4.03	967	786.9	253	-0.70 ± 0.05	-0.72 ± 0.15	21.4	29.0
189-329	M0e	4.48	1000	486.3	315	-0.27 ± 0.06	-0.20 ± 0.08	22.0	29.6
191-350	G8-K5	2.46	1011	530.5	354	-0.03 ± 0.08	0.40 ± 0.06	22.1	29.6
d197-427	M0-M2.5e	0.20	1045	834.7	4273	-0.26 ± 0.02	-0.11 ± 0.02	21.8	30.4
198-222	late-M	...	1056	825.8	359	0.55 ± 0.07	0.19 ± 0.06	22.5	29.8
198-448	M1-M6.5	...	1058	778.1	1348	-0.46 ± 0.03	-0.37 ± 0.04	21.6	29.8
202-228	1084	825.8	651	-0.37 ± 0.04	-0.34 ± 0.06	22.0	29.8
d203-504	1091	746.2	78	0.19 ± 0.14	-0.37 ± 0.14	22.6	29.5
205-330	M0	2.02	1101	371.4	3753	-0.41 ± 0.02	-0.23 ± 0.03	21.7	30.6
205-052	1104	809.9	1907	-0.07 ± 0.03	-0.17 ± 0.03	22.0	30.2
d205-421	cont	...	1107	832.9	60	-0.23 ± 0.15	-0.42 ± 0.23	22.0	28.7
d206-446	M2e	...	1112	832.9	2788	0.20 ± 0.02	-0.03 ± 0.02	22.3	30.5
208-122	K7	0.87	1120	815.2	323	-0.18 ± 0.06	-0.16 ± 0.08	21.8	29.2
212-557	M0.5	...	1139	498.7	307	0.61 ± 0.12	0.70 ± 0.04	23.0	30.4
212-260	M3	3.01	1141	454.5	874	-0.25 ± 0.04	-0.29 ± 0.05	22.1	30.4
213-346	K7	2.09	1149	615.4	4491	-0.43 ± 0.01	-0.25 ± 0.02	21.7	30.5
215-317	M3.5	4.74	1155	514.6	348	-0.36 ± 0.05	-0.58 ± 0.08	21.6	29.4
218-339	K5-K7	3.97	1167	779.8	335	0.33 ± 0.07	0.06 ± 0.06	22.4	29.9
d218-354	G6-K3	1.51	1174	613.6	786	-0.35 ± 0.04	-0.37 ± 0.05	21.7	29.8
221-433	1184	831.1	296	-0.56 ± 0.05	-0.28 ± 0.11	21.3	29.0
224-728	M4.5e	...	1206	801.1	914	-0.39 ± 0.03	-0.27 ± 0.05	21.8	29.8
236-527	1262	822.3	60	0.07 ± 0.27	0.58 ± 0.12	22.5	28.9
237-627	M3	3.21	1263	270.6	29	-0.78 ± 0.14	-0.91 ± 0.75	21.7	28.8

Table 3—Continued

Proplyd	Sp. Type ^a	A_V (mag)	COUP	Exp. ^b (ks)	Counts ^c	HR2 ^d	HR3 ^e	$\log N_H$ ^f (cm $^{-2}$)	$\log L_{t,c}$ ^g (erg s $^{-1}$)
239-510	M1	...	1275	824.1	564	0.02±0.05	-0.07±0.05	22.1	29.7
240-314	1276	790.5	578	0.28±0.06	0.17±0.05	22.3	29.9
242-519	K0-K5e	1.72	1281	820.5	1554	-0.58±0.02	-0.34±0.05	21.3	29.7
d244-440	M0e	0.92	1290	626.0	1930	0.02±0.03	-0.04±0.03	22.2	30.5
245-632	M4-M5	1.39	1291	328.9	406	-0.48±0.05	-0.38±0.08	21.5	29.5
245-502	M1e	...	1293	661.4	20	-0.13±0.36	0.18±0.34	21.9	28.2
247-436	M0e	2.15	1302	774.5	351	-0.11±0.06	0.02±0.07	22.0	29.4
250-439	1313	774.5	94	-0.70±0.08	-0.60±0.29	21.0	28.4
d252-457	1317	680.8	20	0.21±0.34	-0.05±0.32	21.4	28.1
d280-1720	M4	0.64	1404	751.6	618	-0.69±0.03	-0.65±0.16	21.1	29.3
282-458	K6-K8e	...	1409	808.1	6381	-0.02±0.01	-0.06±0.02	22.0	30.7

^aSee Getman et al. 2005a.

^bEffective exposure time.

^cNet photon counts after background subtraction.

^dCOUP X-ray hardness ratio 2, defined as $(C_s - C_m)/(C_s + C_m)$ where C_s is counts in the 0.5–1.7 keV band and C_m is counts in the 1.7–2.8 keV band.

^eCOUP X-ray hardness ratio 3, defined as $(C_m - C_h)/(C_m + C_h)$ where C_m is counts in the 1.7–2.8 keV band and C_h is counts in the 2.8–8.0 keV band.

^fAbsorbing column derived from spectral model fitting.

^gTotal X-ray luminosity in the 0.5–8.0 keV band, corrected for absorption, as derived from spectral model fitting.

Table 4. Statistics of Proplyd X-ray Counterparts

Group ^a	Total No.	$\Delta_X < 1.0''$	$\Delta_X < 0.4''$
candidates	172	112	105
rejected	22	9	8
proplyds	143 ^b	101	94
star	106	90	84
no star	37	11	10
jet(s)	30 ^c	19	19
dark disk	39 ^d	22	19
dark disk, no star	21	4	3 ^e
near-IR src	119 ^f	90	..
no near-IR src	10	1	1 ^g

^aBased on positions and appearances in ACS images; “star” (“no star”) indicates those proplyds with (without) a central star apparent in ACS images.

^bNot including 6 proplyd candidates (3 with COUP counterparts) that lie outside the ACS fields, and not including the jet/disk source d347-1535, which lies outside the COUP field.

^cNot including d347-1535.

^dNot including two proplyds lying outside the COUP field.

^eCOUP IDs: 419, 476, and possibly 948

^fIR source within 0.4'' (except d239-334; IR source found 0.8'' away); 14 proplyd candidates not in VLT field

^gCOUP ID: 695

Table 5. Silhouette Disks Detected in ACS Images

Object	Dimensions ($''$)	R^a	P.A. ($^{\circ}$)	Star?	$\log N_H$ (cm^{-2})	Comments ^b
d053-717	1.1×0.2	5.5	110	Y	22.70	COUP 241; edge-on? (see §4.1)
d072-135	1.0×0.25	4.0	100	N	...	edge-on?
d109-327	0.2×0.1	2.0	160	N	...	
d114-426	2.7×0.7	3.9	30	N	23.73	COUP 419; edge-on? [B2000: $i > 85$ deg]
d121-1925	0.8×0.5	1.6	120	Y	21.57	COUP 460 [B2000: $i = 51$ deg]
d124-132	0.3×0.1	3.0	0	N	...	COUP 476; poor spectral fit
131-046	0.3×0.2	1.5	80:	N	...	
d132-042	0.4×0.25	1.6	85	N	...	
d132-1832	1.5×0.3	5.0	60	N	...	edge-on? [B2000: $i = 75$ deg]
140-1952	0.5×0.5	1.0	..	Y	20.00	COUP 597
d141-520	0.4×0.35	1.1	135	Y	21.16	COUP 604
d143-522	0.4×0.2	2.0	140	N	...	
d147-323	0.25×0.15	1.7	40	Y	22.23	COUP 658
d154-240	0.25×0.10	2.5	90	N	...	
d163-026	0.5×0.15	3.3	160	N	...	edge-on? [B2000: $i > 78$ deg]
d163-222	0.3×0.2	1.5	70	Y	21.20	COUP 799
d165-254	0.4×0.2	2.0	5	N	...	[B2000: $i > 71$ deg]
166-519	??	??	??	N?	...	orientation, dimensions uncertain
d167-231	0.4×0.4	1.0	..	Y	21.62	COUP 825 [B2000: $i < 30$ deg]
d172-028	0.6×0.4	1.5	5	Y	21.35	COUP 865 [B2000: $i = 55$ deg]
d176-543	0.6×0.3	2.0	20	Y	21.43	COUP 901
d177-541	??	??	??	N	...	orientation, dimensions uncertain
d181-247	0.3×0.15	2.0	160	N	...	
d181-825	1.5×0.6	2.5	70	N?	22.78 ^c	COUP 948
d182-332	0.3×0.15	2.0	0	Y?	...	[B2000: $i = 60$ deg]
d182-413	0.5×0.15	3.3	90	N	...	
d183-419	0.3×0.15	2.0	40	N	...	
d183-405	0.7×0.5	1.4	45	Y	21.66	COUP 966 [B2000: $i = 39$ deg]
d191-232	0.3×0.1	3.0	170	N	...	[B2000: $i = 65$ deg]
d197-427	0.6×0.4	1.5	50	Y	21.80	COUP 1045
202-228	0.2×0.15	1.3	45	Y	21.97	COUP 1084
d203-506	0.4×0.2	2.0	15	N	...	[B2000: $i = 67$ deg]
d205-421	0.4×0.3	1.3	60	Y	22.02	COUP 1107
d206-446	0.5×0.3	1.7	70	Y	22.30	COUP 1112
d218-354	1.4×0.6	2.5	70	Y	21.67	COUP 1174 [B2000: $i = 65$ deg]
d218-529	0.4×0.2	2.0	175	N	...	[B2000: $i = 60$ deg]

Table 5—Continued

Object	Dimensions ($''$)	R^a	P.A. ($^{\circ}$)	Star?	$\log N_H$ (cm^{-2})	Comments ^b
d239-334	0.5×0.2	2.5	20	[B2000: $i = 66$ deg]
d253-1536	1.2×0.6	2.0	80	Y?	...	
d280-1720	0.7×0.6	1.2	10	Y	21.10	COUP 1404
d294-606	1.0×0.25	4.0	85	N	...	edge-on? [B2000: $i > 85$ deg]
d347-1535	0.7×0.2	3.5	130	N	...	off COUP FOV

^aRatio of major to minor axes of silhouette disk.

^b[B2000]: included in Table 1 of Bally et al. 2000

^cAbsorbing column inferred for hard spectral component.

Table 6. Jets and Microjets Detected in ACS and/or WFPC2 Images

Object	COUP ID	Star?	Comments ^a
069-600	279	Y	w069-600 [B2000]
d109-327	...	N	HH 510 [B2000]
d110-3035	...	N	
d124-132	476	N	[S2005]
131-247	524	N	HH 511 [B2000]
d132-042	...	N?	dark disk [S2005]
154-324	...	Y	star + jet
157-533	728	Y	HH 512 [B2000]
164-511	803	Y	jet?
165-235	807	Y	HH 513 [B2000]
167-317	826	Y	HH candidate [B2000]
170-337	847	Y	HH 514 [B2000]
d176-543	901	Y	dark disk; HH 515 [B2000]
d177-341	...	Y	HH candidate
d181-825	948	N?	dark disk; Beehive Proplyd; HH 540
d182-413	...	N	dark disk; HH 517 [B2000]
191-350	1011	Y	HH candidate [B2000]
201-534	...	Y	jet?
d203-504	1091	Y	HH 519
d203-506	...	N	dark disk; HH 520 [B2000]
d206-446	1112	Y	dark disk; HH 521 [B2000]
208-122	1120	Y	jet?
d218-354	1174	Y	dark disk; HH candidate [B2000]
d218-529	...	N	
d239-334	HH 522; COUP 1268 at companion [B2000]
d244-440	1290	Y	HH 524 [B2000]
247-436	1302	Y	HH 525 [B2000]
d252-457	1317	Y	HH 526 [B2000]
d253-1536	...	Y?	HH 668 [S2005]; COUP 1316 at companion
282-458	1409	..	HH 527 [B2000]
d347-1535		N	dark disk, extensive bipolar jets [S2005]

^a[B2000]: listed in Table 3 of Bally et al. 2000; [S2005]: listed in Smith et al. 2005

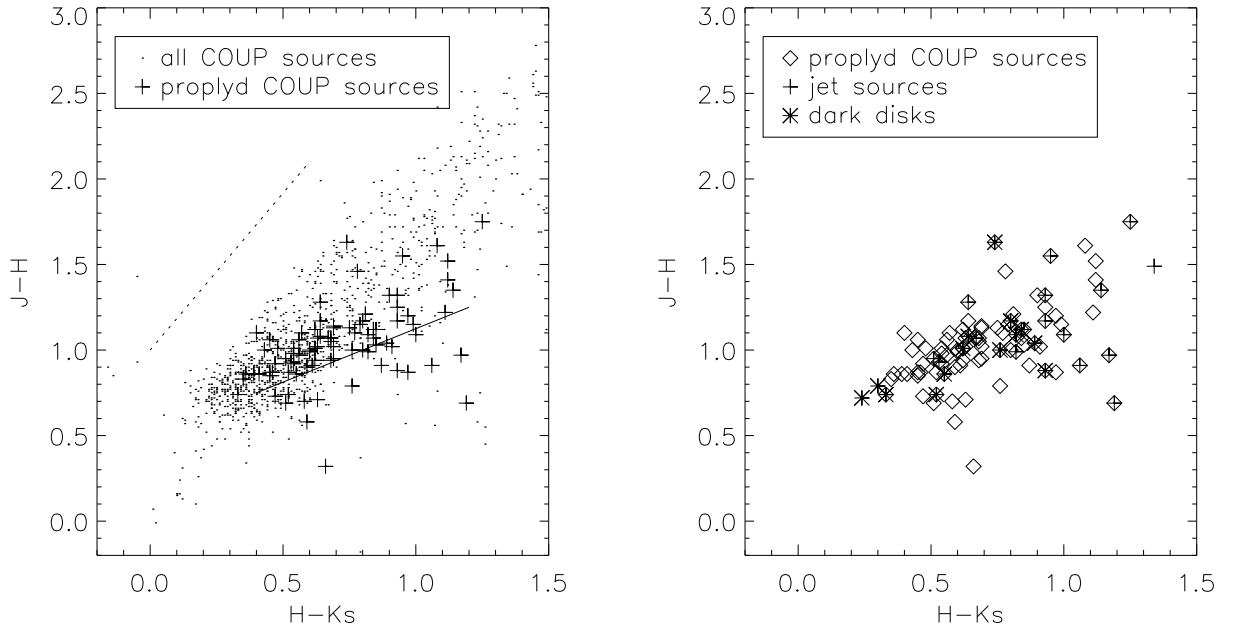


Fig. 1.— $J - H$ vs. $H - K_s$ color-color diagrams for Table 1 objects with available (VLT or 2MASS) near-infrared photometry. Left: near-infrared colors of Table 1 COUP sources (crosses) overlaid on a plot of the near-infrared colors of all COUP sources for which near-infrared photometry is available. The dotted line indicates the reddening vector for $A_V = 10$, and the solid line indicates the locus of near-infrared colors of classical T Tauri stars in Taurus (Meyer et al. 1997). Some very heavily absorbed COUP sources lie off the right edge of the plot. Right: near-infrared colors for proplyd sources only, with jet sources (crosses) and silhouette disk proplyds (asterisks) highlighted (see §§4, 5).

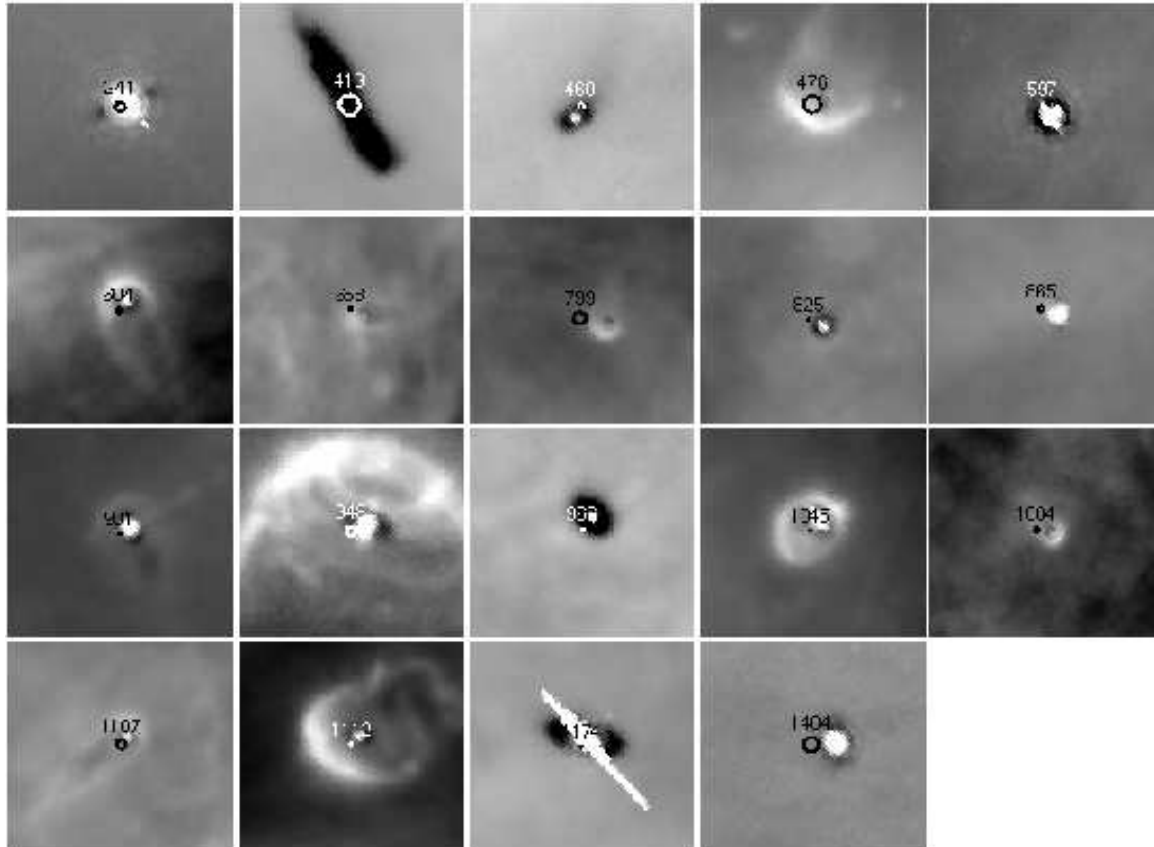


Fig. 2.— HST/ACS images of silhouette disk proplyds with COUP X-ray counterparts. Top row, from left to right: d218-354 (COUP 241), d114-426 (419), d121-1925 (460), 140-1952 (597), d141-520 (604); second row: d147-323 (658), d163-222 (799), d167-231 (825), d172-028 (865), d176-543 (901); third row: d181-825 (948), d183-405 (966), d197-427 (1045), 202-228 (1084), d205-427 (1045); bottom row: d205-421 (1107), d206-446 (1112), d218-354 (1174), d280-1720 (1404). The field of view in each displayed ACS image region is $2.7'' \times 2.7''$ with N up and E to the left. In each image, the COUP source position is indicated by a circle whose radius is equal to the positional uncertainty for that source, as determined from X-ray source detection; there is an additional random scatter of $\sim 0.2''$ in COUP source positions (see Getman et al. 2005a, their Fig. 9).

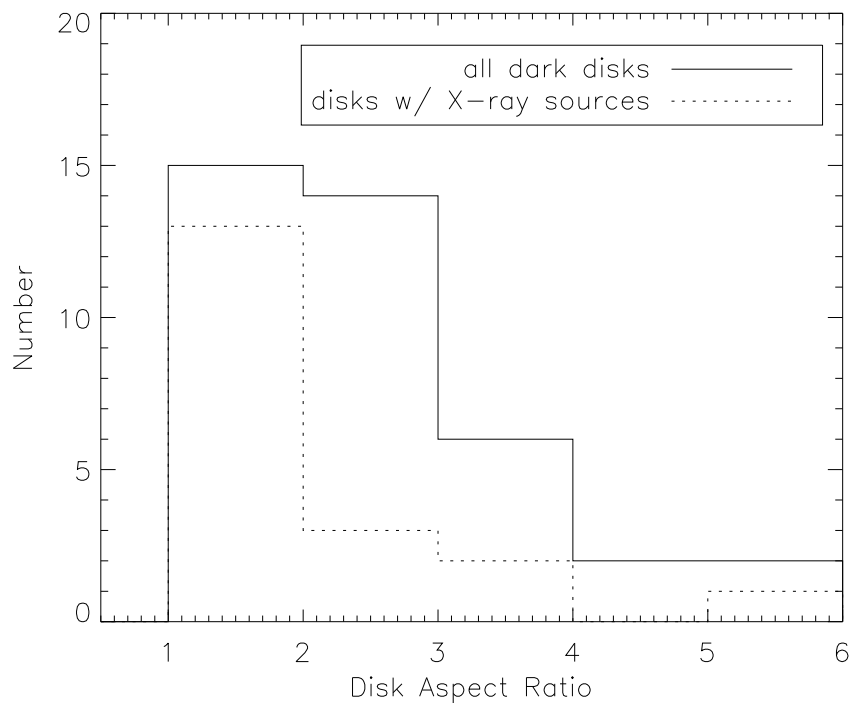


Fig. 3.— Histograms of number of silhouette disks vs. aspect ratio, for silhouette proplyds listed in Table 5. The solid line indicates the total number of disks in each aspect ratio bin, while the dotted line indicates only those disks harboring X-ray sources.

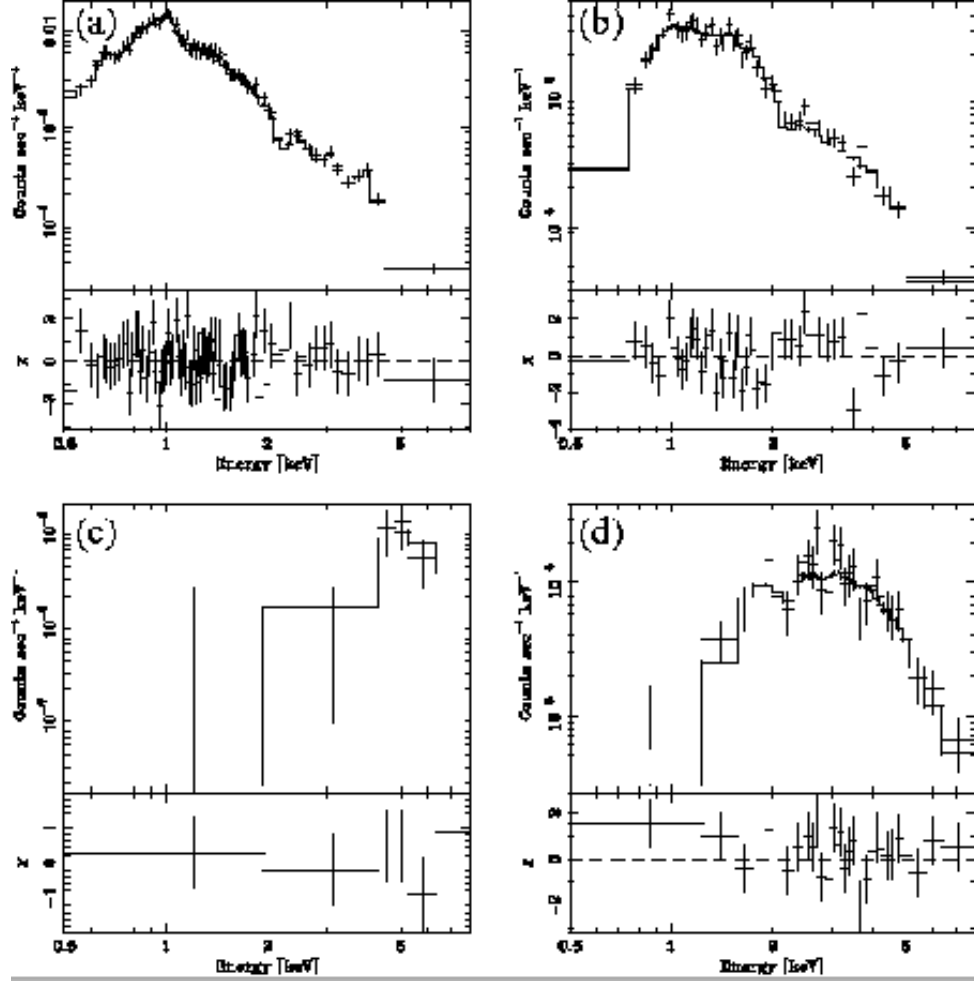


Fig. 4.— COUP X-ray spectra of representative sources associated with silhouette disk proplyds. COUP 597 (panel a) and COUP 825 (panel b) are X-ray counterparts to presumably nearly face-on disks, i.e., silhouette disks with small aspect ratios, while COUP 419 (panel c) and COUP 241 (panel d) are counterparts to silhouette disks with the largest aspect ratios. For each source, X-ray spectral data (and associated uncertainties) are indicated by crosses, the histogram represents the best-fit spectral model, and residuals of the fit are indicated in the bottom panel (see Getman et al. 2005a).

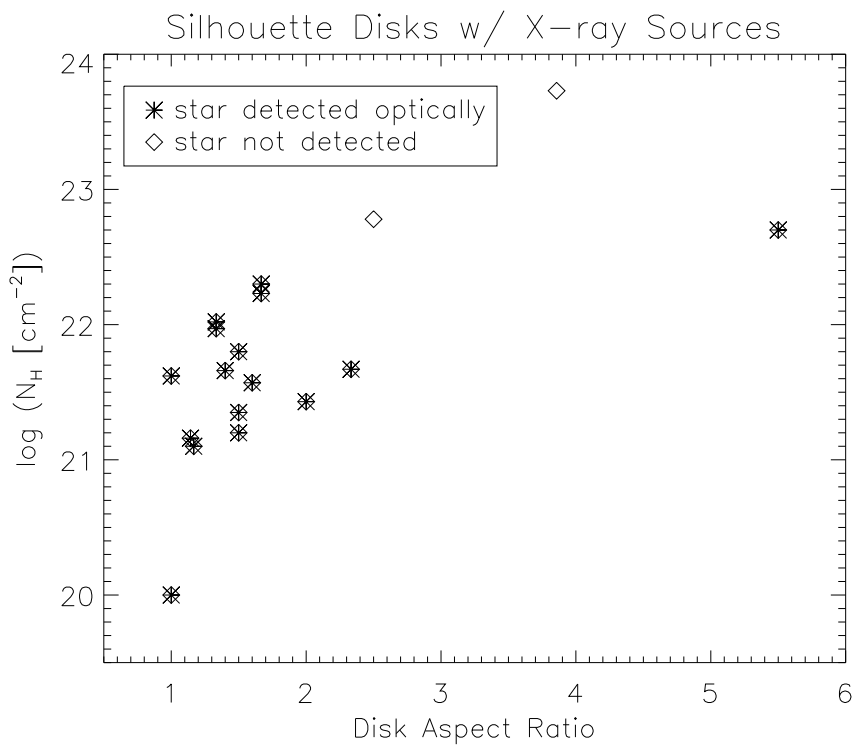


Fig. 5.— X-ray-inferred column density, $\log N_H$ (cm^{-2}), vs. disk aspect ratio, for silhouette disk proplyds listed in Table 5. Asterisks indicate proplyds with optically detected central stars. The bright central star detected within the silhouette disk with the largest aspect ratio, d053-717, may not be the source of X-ray emission (see §4.1).

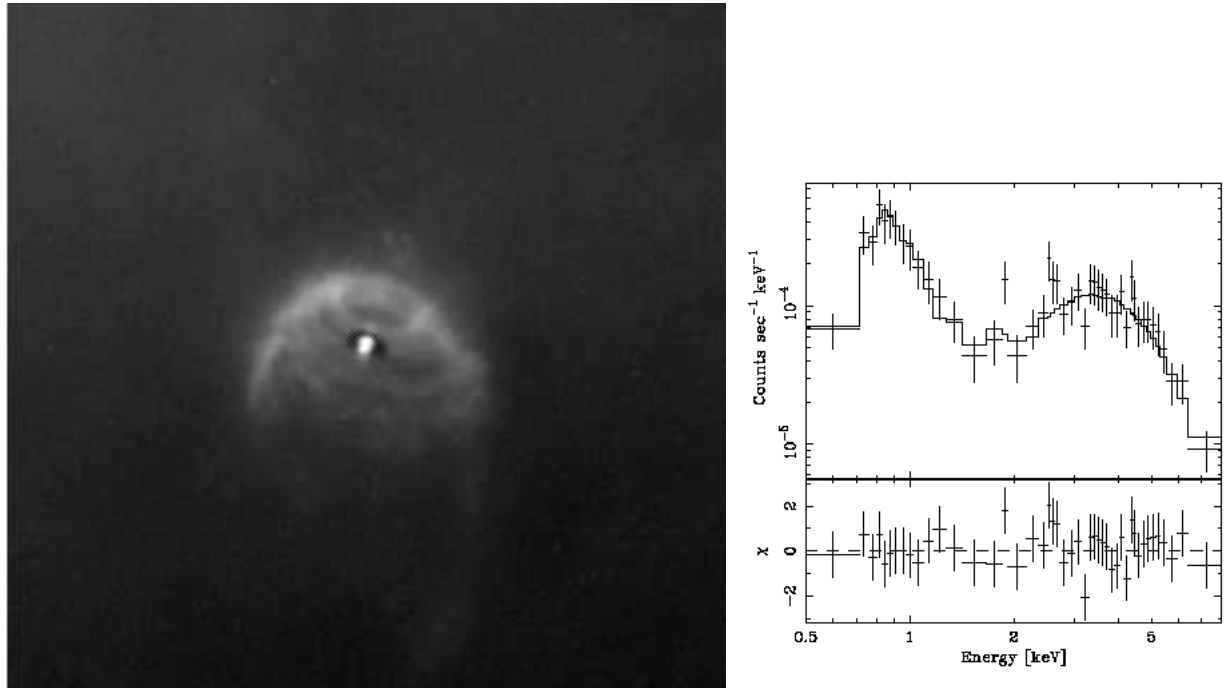


Fig. 6.— Left: HST/ACS image of the Beehive Proplyd (d181-825), associated with COUP 948. The field of view $11'' \times 11''$ with N up and E to the left. Right: COUP X-ray spectrum of COUP 948. Note the double-peaked X-ray spectral energy distribution.

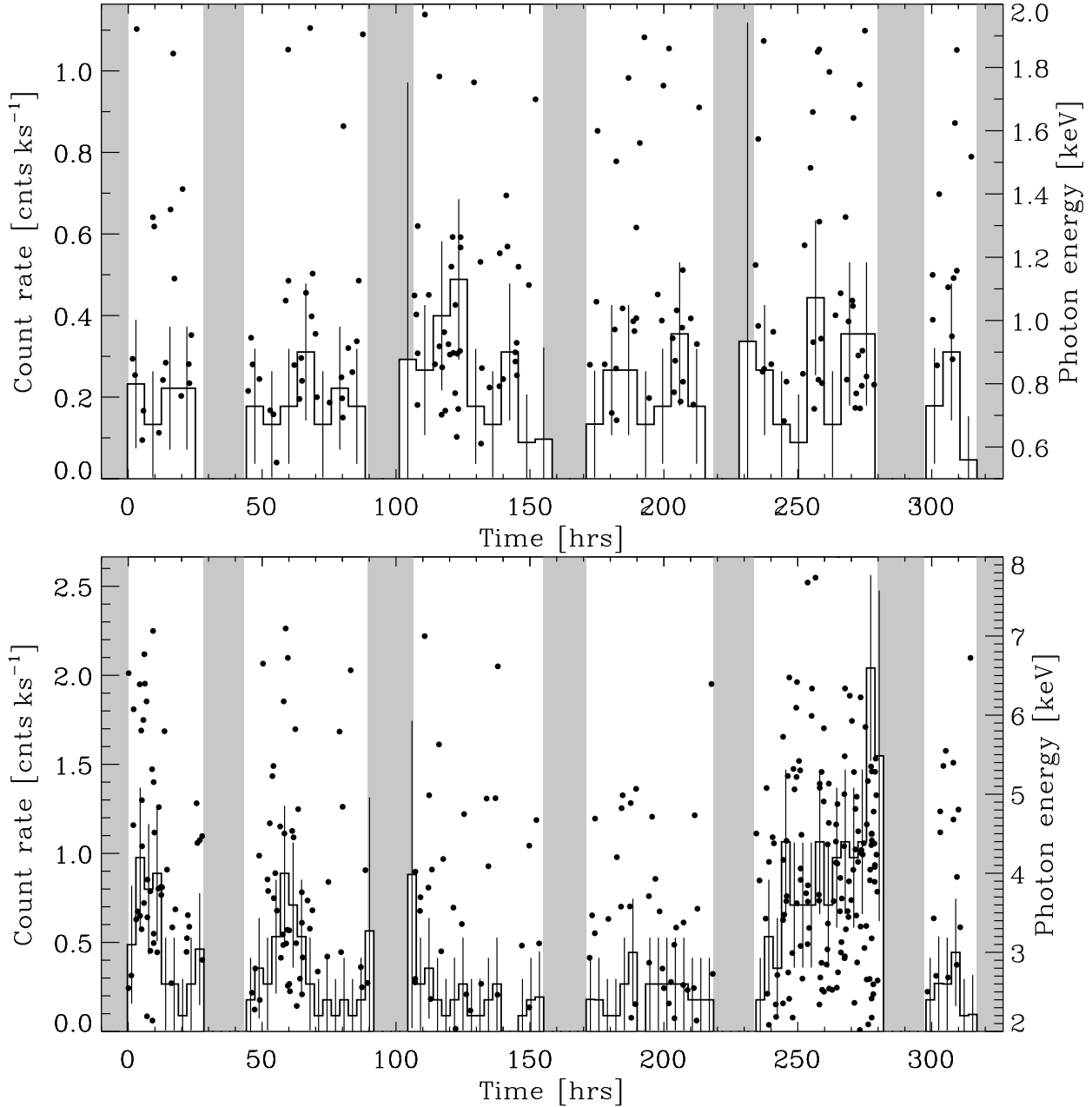


Fig. 7.— Light curves of COUP 948, which is associated with the Beehive Proplyd (d181-825). Top: soft band (0.5–2.0 keV). Bottom: hard band (2.0–8.0 keV). In each plot, the histogram indicates the integrated counts within the band, while the points indicate the arrival times and energies of individual photons. The grey bands indicate gaps in temporal coverage during the 838 ks COUP observation.

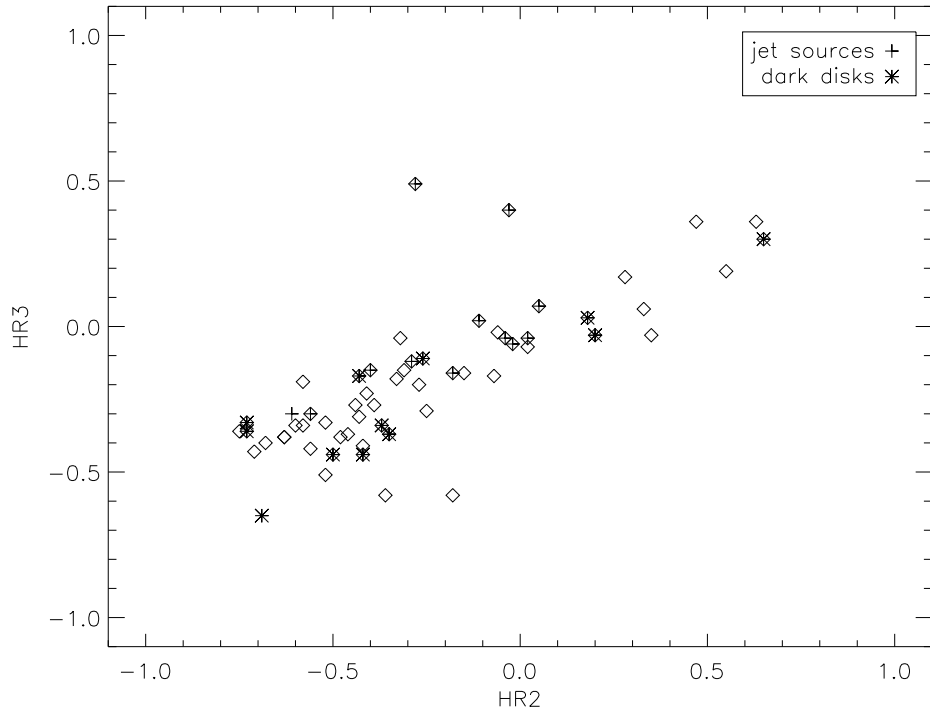


Fig. 8.— COUP X-ray hardness ratios HR2 and HR3 (see Table 3) of proplyd COUP sources (diamonds), with hardness ratios of silhouette disk proplyds (“dark disks”) and jet sources indicated by asterisks and crosses, respectively. Only sources with uncertainties ≤ 0.1 in HR2 and HR3 are plotted. The two crosses at the upper left of the diagonal locus of points are the COUP counterparts to jet sources d181-825 (COUP 948, which has the largest value of HR3 of any source in the Figure) and 191-350 (COUP 1011).

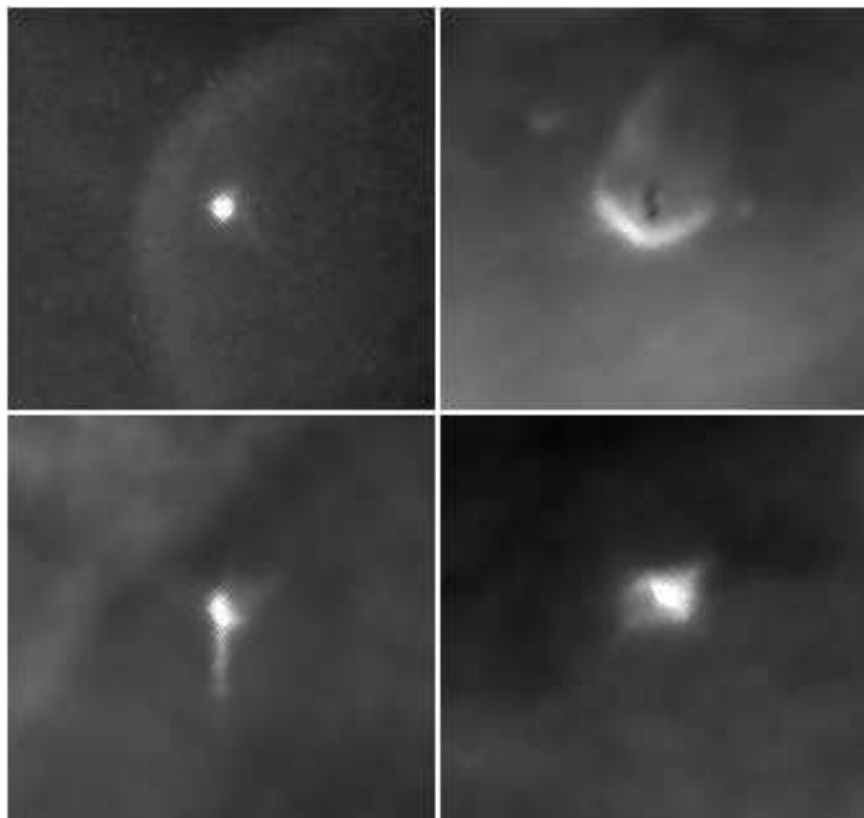


Fig. 9.— HST/ACS images of jet sources whose X-ray hardness ratios appear anomalous. From top to bottom, left to right: 069-601, d124-132, 131-247, and 191-350 (COUP X-ray counterparts are 279, 476, 524, and 1011, respectively). The field of view in each case is $4.2'' \times 4.2''$, with N up and E to the left.

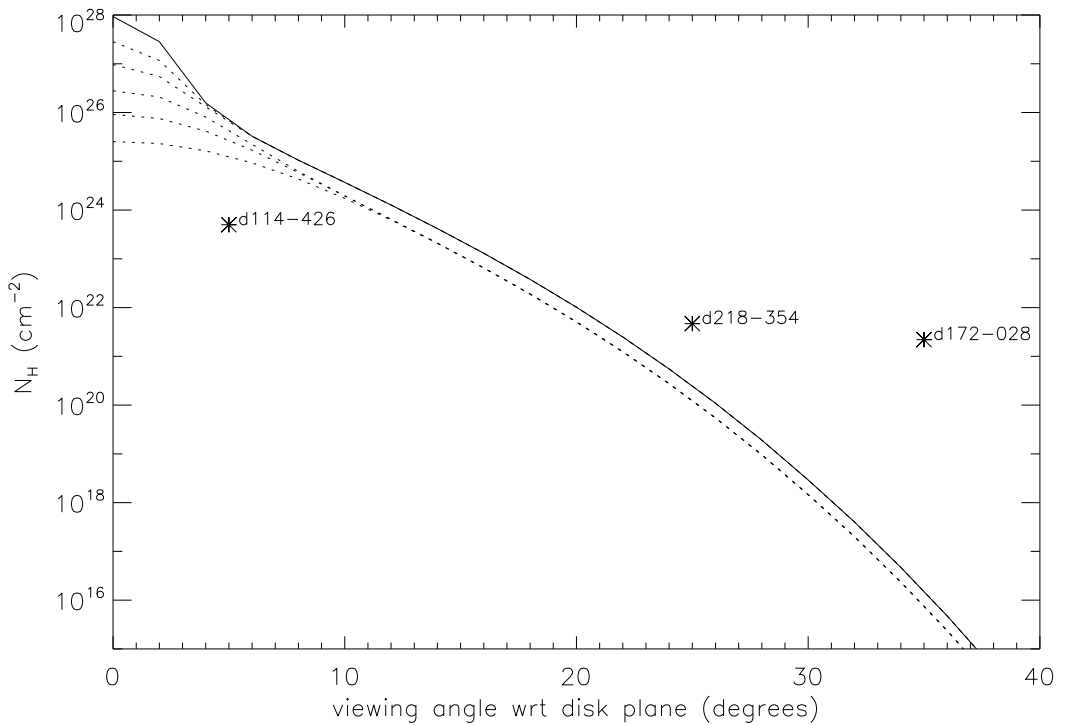


Fig. 10.— Model distribution of N_{H} vs. i obtained from the circumstellar disk model. The top-to-bottom curves represent a range of assumed inner radii for the disk, from 0.03 AU to 10 AU. The estimated inclinations and corresponding N_{H} values for three representative proplyds are indicated in the plot; the disk viewing angles for these sources are based on inclination estimates listed in Bally et al. (2000).